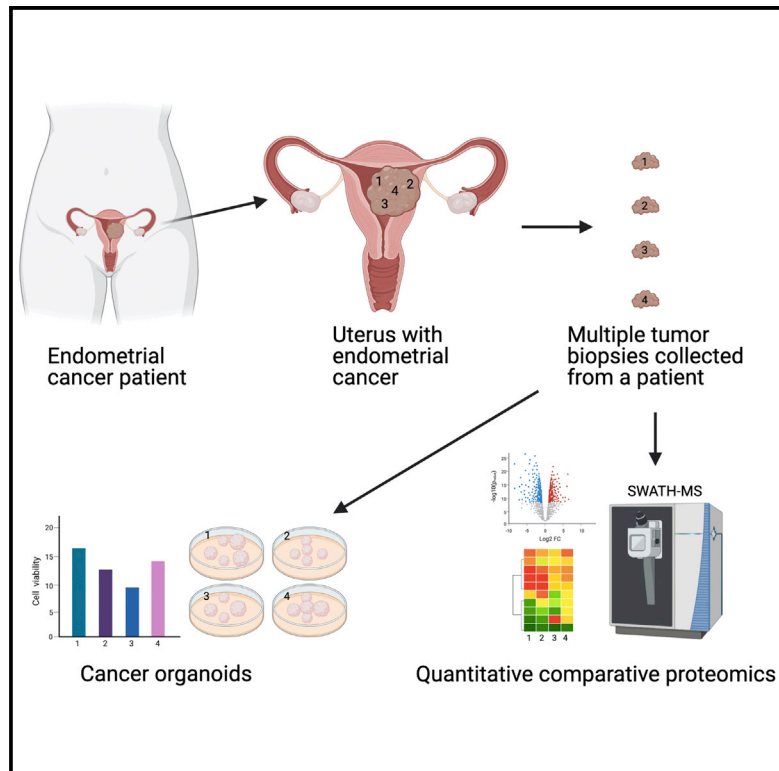


Proteomic and functional characterization of intra-tumor heterogeneity in human endometrial cancer

Graphical abstract



Authors

M. Fairuz B. Jamaluddin, Yi-An Ko, Arnab Ghosh, ..., Pravin Nahar, Kenneth Jaaback, Pradeep S. Tanwar

Correspondence

pradeep.tanwar@newcastle.edu.au

In brief

Despite significant investment in the molecular analysis of solid tumors, few preclinical findings translate to patients. Tumor heterogeneity is suspected as one primary reason for the targeted therapy failure. Here, Jamaluddin et al. describe endometrial cancer intra-tumor heterogeneity using quantitative proteomics and patient-derived organoids.

Highlights

- Proteomic analysis of endometrial cancer intra-tumor heterogeneity
- Identification of potential biomarkers of tumor volume and invasion
- Protein signatures correlate with pre-and postmenopausal cancers
- Patient-derived organoids capture endometrial cancer heterogeneity



Article

Proteomic and functional characterization of intra-tumor heterogeneity in human endometrial cancer

M. Fairuz B. Jamaluddin,^{1,2,3} Yi-An Ko,^{1,2,3} Arnab Ghosh,^{1,2,3} Shafiq M. Syed,^{1,2,3} Yvette Ius,⁴ Rachel O'Sullivan,⁴ Jacob K. Netherton,^{2,3} Mark A. Baker,^{2,3} Pravin Nahar,⁵ Kenneth Jaaback,⁴ and Pradeep S. Tanwar^{1,2,3,6,*}

¹Global Centre for Gynecological Diseases, University of Newcastle, LS236, University Drive, Callaghan, NSW 2308, Australia

²School of Biomedical Sciences and Pharmacy, College of Health, Medicine and Wellbeing, University of Newcastle, Callaghan, NSW 2308, Australia

³Hunter Medical Research Institute, New Lambton Heights, NSW 2305, Australia

⁴Hunter New England Centre for Gynecological Cancer, John Hunter Hospital, New Lambton Heights, NSW 2305, Australia

⁵Department of Maternity and Gynecology, John Hunter Hospital, New Lambton Heights, NSW 2305, Australia

⁶Lead contact

*Correspondence: pradeep.tanwar@newcastle.edu.au

<https://doi.org/10.1016/j.xcrm.2022.100738>

SUMMARY

Endometrial cancer is one of the most frequently diagnosed gynecological cancers worldwide, and its prevalence has increased by more than 50% over the last two decades. Despite the understanding of the major signaling pathways driving the growth and metastasis of endometrial cancer, clinical trials targeting these signals have reported poor outcomes. The heterogeneous nature of endometrial cancer is suspected to be one of the key reasons for the failure of targeted therapies. In this study, we perform a sequential window acquisition of all theoretical fragment ion spectra (SWATH)-based comparative proteomic analysis of 63 tumor biopsies collected from 20 patients and define differences in protein signature in multiple regions of the same tumor. We develop organoids from multiple biopsies collected from the same tumor and show that organoids capture heterogeneity in endometrial cancer growth. Overall, using quantitative proteomics and patient-derived organoids, we define the heterogeneous nature of endometrial cancer within a patient's tumor.

INTRODUCTION

Endometrial cancer (EC) is currently the most common cancer of the female genital tract in developed countries.¹ The incidence of EC has continued to increase over more than 50% during the last two decades, with 66,570 new cases and 12,940 deaths recorded in 2021 in the United States alone.^{2,3} The main hallmark symptom of EC is abnormal uterine bleeding, which is present in more than 90% of patients.⁴ Treatment options for patients with EC are limited to surgery (hysterectomy and bilateral salpingo-oophorectomy) followed by adjuvant therapy (chemotherapy or hormonal agents) depending on the clinical and histopathological characteristics of the disease.^{5,6} While primary surgical treatment is beneficial in most patients with EC, about 15%–20% of patients are still likely to develop the recurrent disease even if no symptoms of advanced or metastatic disease are present at the time of diagnosis.⁷ According to the International Federation of Gynecology and Obstetrics (FIGO), the chance of recurrence is 10%–20% in stages I–II and 50%–70% in stages III–IV.⁸ Therefore, a better understanding of EC is urgently needed to develop unique drug targets and new treatment strategies.

Recent genomic analysis has resulted in the identification of four different clusters of human EC. These include (1) polymerase ϵ (POLE) ultramutated, (2) microsatellite instability (MSI) hypermutated, (3) copy-number low, and (4) copy-number high.⁹ Activating genetic alterations in the PI3K-mTOR pathway are commonly present in human patients with EC, and similar alterations in mouse models result in the development of ECs that are histologically, phenotypically, and molecularly similar to human EC.^{9–11} Suppression of PI3K-mTOR signaling using rapalogs in human cancer cells and mouse models results in the inhibition of growth of EC,¹² providing a strong rationale for testing rapalogs in human patients with EC. Despite this evidence, clinical trials with rapalogs have reported a modest response in human patients, and alterations in *PTEN* and *PIK3CA* are unable to predict response to rapalogs.^{13,14} Data from preclinical and clinical trials suggest that ECs initially respond to rapalog treatments, resulting in stable disease. However, tumors stop responding over time and overcome the inhibition of PI3K-mTOR signaling.¹⁵ Multiregional sequencing of normal human endometrium and endometriotic lesions revealed distinct mutations, including alterations in *PIK3CA* and *PTEN*, in different glands and in discrete regions of the same tissue, suggesting that endometrial cells are



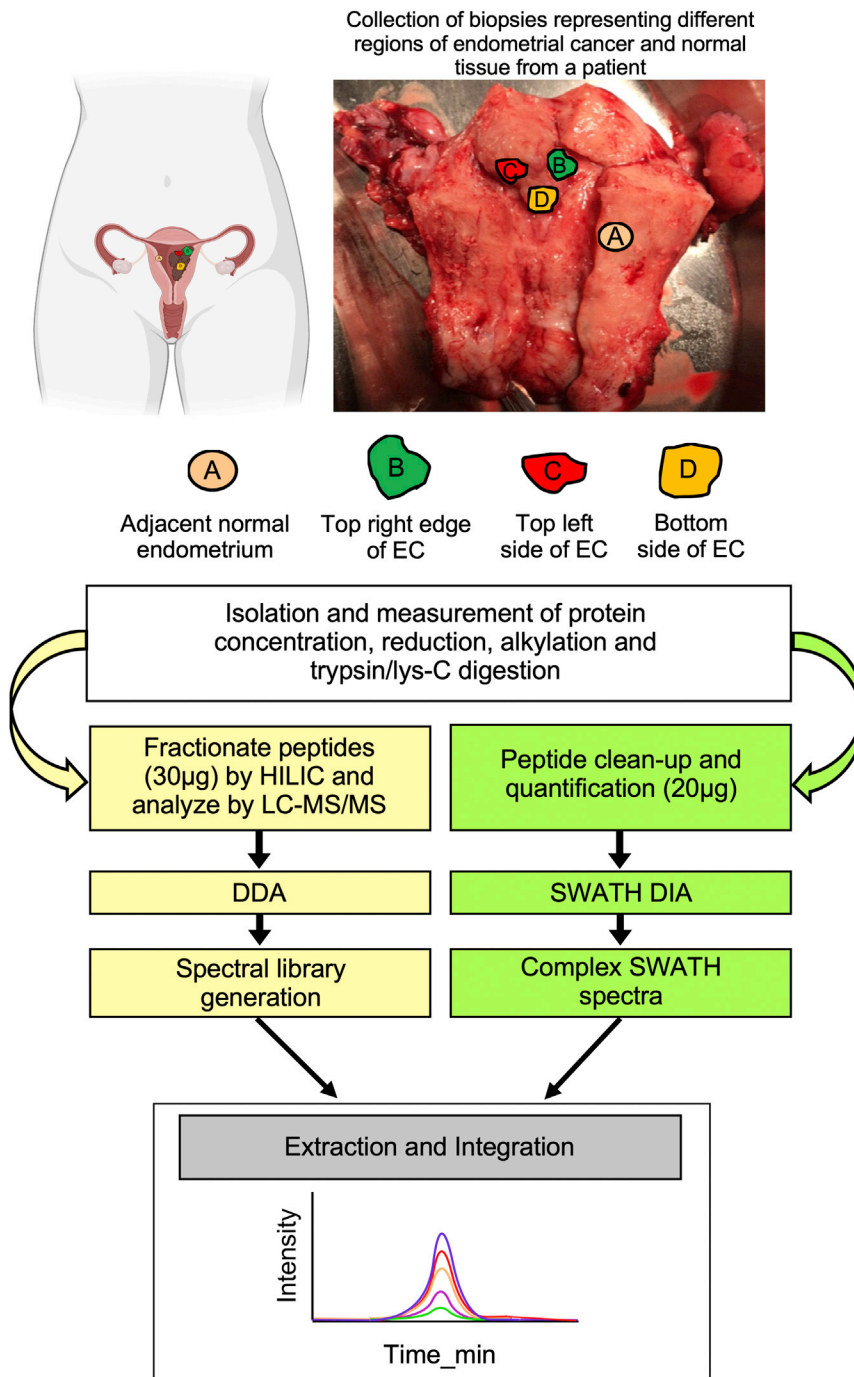


Figure 1. Schematic representation for the SWATH-based proteomics workflow

(A–D) Adjacent normal endometrium (A) and three (B–D) tumor samples were isolated in different sites of the endometrium cancer region from individual patients before protein digestion and LC-MS/MS analysis. Each peptides sample was injected separately in a data-dependent acquisition (DDA) mode, to generate a spectral library, and in a SWATH (DIA) mode. The spectral library generated from the DDA runs was used by Peakview and Markerview to extract the peptide and the quantification information on each of the SWATH runs. Experimental procedures are described in the STAR Methods.

understood regarding the heterogeneous nature of EC, particularly at the proteomic level.

In the present study, we isolated tumor biopsies from different regions of patient EC tissue. Next, we performed a sequential window acquisition of all theoretical fragment ion spectra (SWATH)-based comparative analysis to profile the protein content in each core area within patient EC tissue. SWATH-mass spectrometry (MS) reproducibly measures the same peptides across all samples and has emerged as a versatile tool for high quantitative accuracy and in-depth analysis of a large number of proteins from complex samples.¹⁹ By using this approach, we have characterized the protein heterogeneity within the same patient with EC. We have also developed organoids from multiple regions of the cancer tissue within a patient and showed differences in the growth of these EC organoids.

RESULTS

Proteomic analysis reveals heterogeneous protein expression profiles in patients with EC

To characterize EC heterogeneity at the proteomic level, we compared the protein composition from each different region of EC tissue samples derived from individual patients (Figure 1). The details of the indi-

genetically heterogeneous.^{16,17} This heterogeneity might contribute to the poor response observed in clinical trials for many single agent-based targeted therapies and the evolution toward drug resistance. The simultaneous presence of multiple subclones in a tumor is one of the major challenges for developing targeted therapies against EC. Intra-tumor heterogeneity in EC may influence the course of the disease, affect patient survival, and impact treatment decision-making.¹⁸ Together, little is

vidual patients and their clinical history are shown in Table 1. The selected cases were representative of the patients with EC with regard to age, tumor type, and FIGO stage. We first isolated protein from tumor tissue samples obtained from approximately 2–4 sites of EC and digested the EC proteins into peptides for subsequent liquid chromatography-tandem MS (LC-MS/MS) analysis (2–4 tumor samples per patient; total n = 63 tumors from 20 patients; Figure 1). We then used a label-free SWATH-MS strategy

Table 1. Clinical characteristics of patients

Patient index	Age (years)	Tumor type	Grade	Site of tumor	Size	Myometrial invasion (%)	Operative specimen
1	69	endometrioid carcinoma	FIGO grade 2	fundus, right side	25 × 18 × 15 mm	47.8	simple hysterectomy, bilateral salpingo-oophorectomy, sentinel nodes
2	69	endometrioid carcinoma	FIGO grade 1	fundus, cornu	50 × 50 × 20 mm (3 dimensions for macroscopic tumors only)	47.5	hysterectomy and bilateral salpingo-oophorectomy, lymph nodes
3	50	endometrioid carcinoma	FIGO grade 2	fundus, cornu, isthmus	40 × 18 × 15 mm (3 dimensions for macroscopic tumors only)	16.67	simple hysterectomy, bilateral salpingo-oophorectomy
4	60	endometrioid carcinoma	FIGO grade 2	fundus and the right cornu	18 × 15 × 13 mm at the fundus (macroscopic measurement)	37.5	total abdominal hysterectomy and right salpingo-oophorectomy
5	72	endometrioid carcinoma	FIGO grade 1	fundus to lower uterine segment and right cornu	40 × 25 × 10 mm	50	simple hysterectomy, including bilateral oophorectomy (previous bilateral salpingectomy)
6	70	endometrioid carcinoma	FIGO grade 1	fundus and cornu	microscopic	29.09	simple hysterectomy, bilateral salpingo-oophorectomy
7	51	endometrioid carcinoma	FIGO grade 1	endometrial cavity	microscopic	8.3%	uterus, tubes, ovaries
8	43	endometrioid carcinoma	FIGO grade 1	fundus to mid portion of endometrial cavity	50 × 38 × 20 mm	–	simple hysterectomy, bilateral salpingo-oophorectomy, bilateral sentinel external iliac lymph nodes
9	62	endometrioid carcinoma	FIGO grade 1	scattered foci microscopic	not measurable, microscopic only	15.38	simple hysterectomy, bilateral salpingo-oophorectomy
10	47	endometrioid carcinoma	FIGO grade 1	fundus, cornu, isthmus, all	microscopic	–	simple hysterectomy, bilateral salpingo-oophorectomy
11	70	endometrioid carcinoma	FIGO grade 2	entire endometrial surface	44 mm supero-inferior, 40 mm left to right, and 26 mm	12.5	simple hysterectomy, bilateral salpingo-oophorectomy, nodes, vulvar biopsies
12	58	endometrioid carcinoma	FIGO grade 2	entire endometrial cavity	80 × 65 × 60 mm	100	simple hysterectomy, bilateral salpingo-oophorectomy, nodes, peritoneal cyst
13	75	serous papillary carcinoma associated with endometrial intraepithelial carcinoma (EIC)	High grade	fundus, cornu, isthmus, all	35 × 20 × 6 mm (for macroscopic tumors only)	47.06	simple hysterectomy, bilateral salpingo-oophorectomy, nodes, omentectomy, peritoneal cytology
14	51	endometrioid carcinoma	FIGO grade 1	lower body	microscopic	–	simple hysterectomy, bilateral salpingo-oophorectomy, nodes, omentectomy, peritoneal cytology
15	60	endometrioid carcinoma	FIGO grade 2	fundus	19 × 6 × 4 mm	38.46	simple hysterectomy, bilateral salpingo-oophorectomy

(Continued on next page)

Table 1. Continued

Patient index	Age (years)	Tumor type	Grade	Site of tumor	Size	Myometrial invasion (%)	Operative specimen
16	82	endometrial carcinoma	FIGO grade 1	fundus and the right cornu	microscopic (3 mm)	-	simple hysterectomy, bilateral salpingo-oophorectomy
17	71	serous endometrial carcinoma	high grade	fundus, cornu	microscopic	-	simple hysterectomy, bilateral salpingo-oophorectomy
18	52	endometrial carcinoma	FIGO grade 1	both cornua and adjacent fundus and corpus	10 mm	20	simple hysterectomy, bilateral salpingo-oophorectomy
19	67	endometrial carcinoma	FIGO grade 1	fundus, cornu, isthmus, all	53 x 15 x 15 mm	8.69	simple hysterectomy, bilateral salpingo-oophorectomy
20	84	endometrial carcinoma	FIGO grade 1	fundus, cornu, corpus	50 x 42 x 7 mm	46.15	uterus, cervix, uterine tubes, and ovaries

to quantify and compare proteins in different areas within EC tissue. For the SWATH analysis, a spectral library of 2,175 proteins was created with a false discovery rate (FDR) <1% from the 15 fractions with the data-dependent acquisition (DDA) method on a TripleTOF q6600 mass spectrometer (Figure S1; Table S1). We then plotted Venn diagrams to check the degree of overlapping proteins expressed within each site of the EC region in a single patient. From the Venn diagrams, a combined total of 1,447, 1,587, 1,464, 1,769, 1,521, 1,311, 916, 1,665, 1,356, 1,345, 1,221, 1,651, 1,567, 1,481, 1,205, 1,670, 1,112, 1,354, 1,317, and 1,518 unique proteins were identified in multiple EC tissues in the twenty patients, respectively. Proteomic analysis of EC in patient 1 led to the identification of up to 1,447 proteins, and 65, 43, and 28 proteins are uniquely present in samples EC 1.1, EC1.2, and EC1.3, respectively (Figure 2). Altogether, these 136 proteins represent promising biomarkers and explain the diversity of protein profile of EC, as they are found in a single EC location but are not detected in other locations within the same tumor. Comprehensive data (including accession number, gene ID, and protein length: number of amino acids) of identified proteins found in the different sites of EC from patient 1 are listed in Table S2.

We next analyzed endometrial heterogeneity in patient 2 (samples EC 2.1, EC 2.2, EC 2.3, and EC2.4) in which tumor cells were located throughout the uterine cavity, and we detected a total of 1,587 proteins (Figure 2). More specifically, we highlighted the differentially expressed proteins that belong to each region, and they contained 36 proteins in sample EC 2.1, 22 proteins in EC 2.2, 16 proteins in EC 2.3, and 12 proteins in EC 2.4 (Figure 2; Table S2).

In an analysis of patient 3, we compared the protein composition of sample EC 3.1 that is positioned specifically at the edge of the tumor versus sample EC 3.2 that is located in middle of tumor and identified 1,464 proteins altogether (Figure 2). Of these 1,464 proteins, 144 proteins were not detected in the central region of the tumor (sample EC3.2) (Figure 2). We further validated the remaining 54 tumors from 17 patients and found that the multiple tumors within all independent patients also contained heterogeneous protein expression (Figure 2). Overall, our proteomic analysis highlighted that tumor tissue samples collected from different sites of EC within the same patient can harbor diverse protein profiles, probably representing different clones of cells forming these tumors.

Proteomic changes in tumors with patient age and tumor size

We next investigated whether changes in tumor proteome were correlated with patient age or tumor characteristics. Age is a significant risk factor for EC development, and significant changes in tumor local and endocrine environment occur with age.^{20,21} Menopause in women occurs at an average of 51 years of age.²² We detected a total of 1,985 proteins in pre- and postmenopausal patients with EC and found that 5.8% of proteins were exclusively higher in post- compared with premenopausal patients (Figure 3A). ECs in postmenopausal patients are usually derived from atrophic endometrium, and their growth is independent of hormones.²⁰ 116 proteins that are exclusively present in postmenopausal ECs could potentially represent cancer drivers involved in the pathogenesis of this disease in aged women

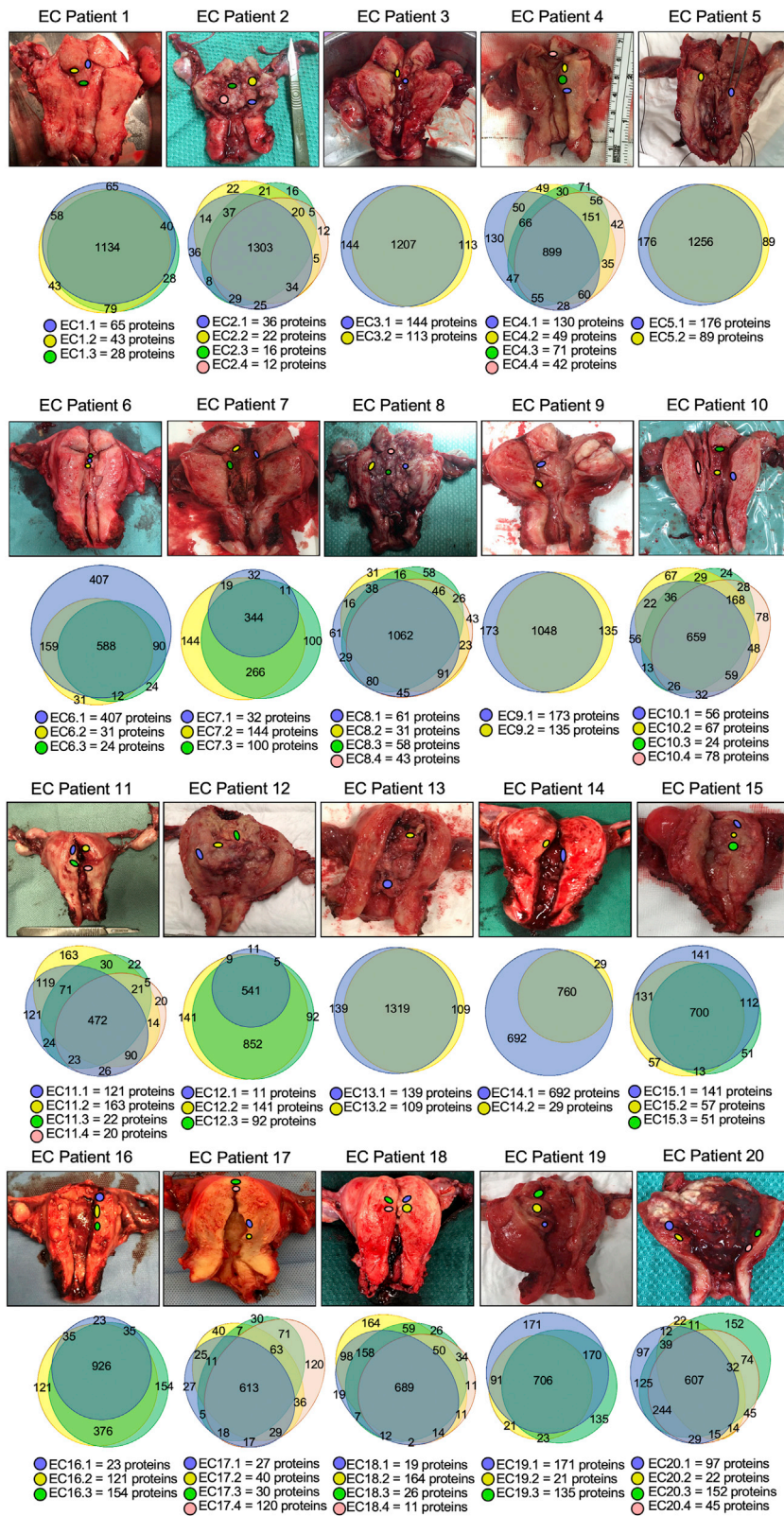


Figure 2. Intra-tumor heterogeneity proteomic profile of patients with endometrial cancer
 Venn diagram illustrating the number of exclusive proteins found in each site within the same tumor from individual patients (n = 63 biopsies from 20 patients). The color code in the Venn diagram corresponds to the isolated site of the endometrial cancer region (see gross surgical images). Comparison in the number of protein identification at FDR < 1%.

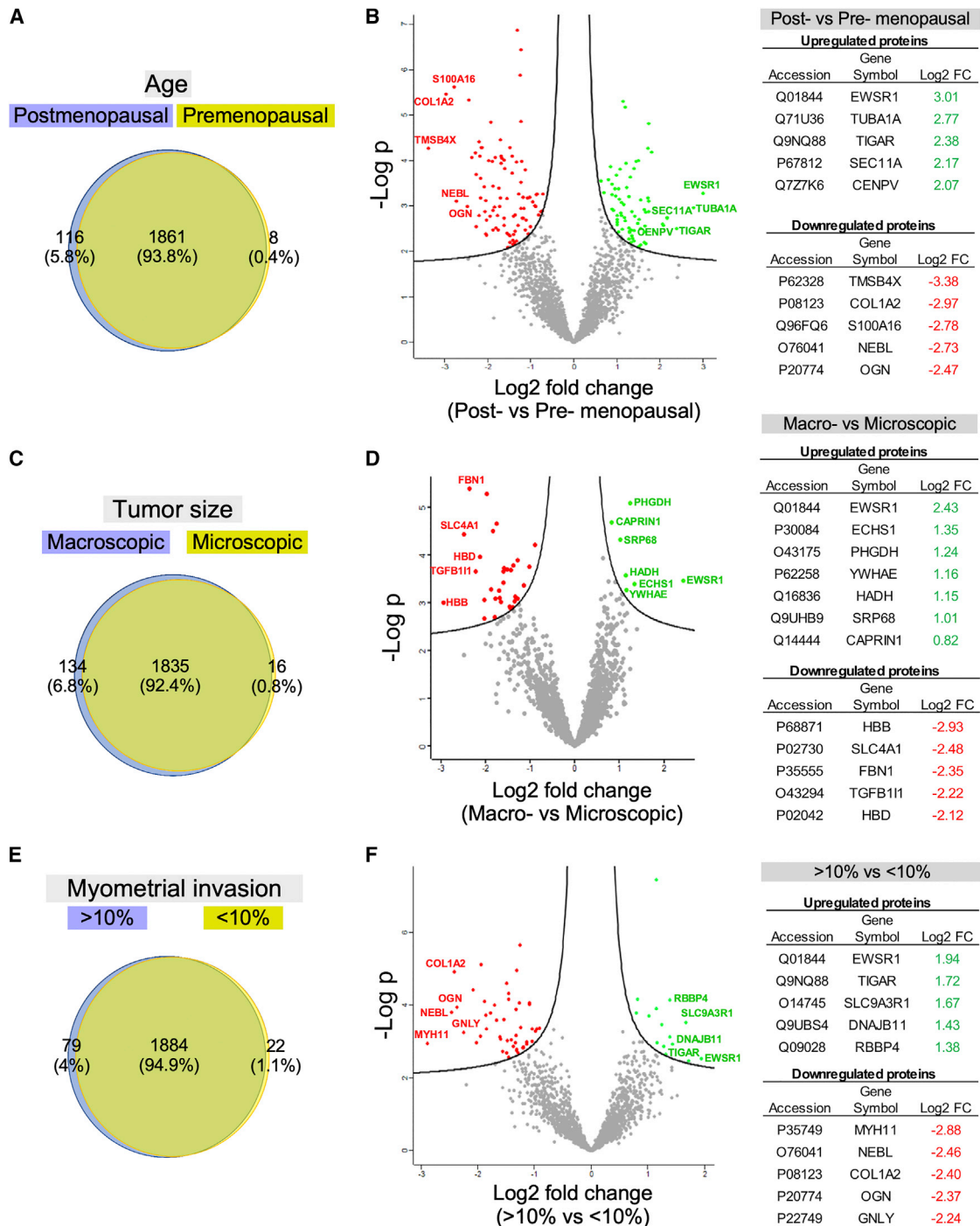


Figure 3. Comparison of quantifiable proteins by SWATH in patients with endometrial cancer

(A, C, and E) Venn diagram depicts overlapped and unique quantifiable proteins identified in patients with endometrial cancer (EC) based on menopausal status, tumor size, and the depth of myometrial invasion.

(B, D, and F) Volcano plots showing the difference of fold change (x axis) and significance of the difference (y axis) in patients with EC between pre- and postmenopausal group, tumor sizes, and myometrial invasion. Proteins that pass a p value threshold for either up- or down-regulated expression are highlighted in green and red, respectively. The top significant up- and down-regulated proteins associated with respective categories are shown in the table.

(Figure 3A). Volcano plot analysis detected 74 statistically significant up-regulated proteins in post- compared with premenopausal patients (Figure 3B). Here, we have highlighted the top five significant up-regulated proteins, and these are RNA-binding protein Ewing sarcoma breakpoint region 1 (EWSR1; log₂ fold change [FC] = 3.01, p = 0.0005); tubulin alpha-1A chain (TUBA1A; log₂FC = 2.77, p = 0.001); fructose-2,6-bisphosphatase TIGAR (TIGAR; log₂FC = 2.38, p = 0.003); signal peptidase complex catalytic subunit SEC11A (SEC11A; log₂FC = 2.17, p = 0.001); and centromere protein V (CENPV; log₂FC = 2.07, p = 0.002) (Figure 3B). We also examined the proteins that were significantly down-regulated in postmenopausal women (91 proteins; Table S2), and the top five candidates are thymosin beta-4 (TMSB4X; log₂FC = -3.38, p = 0.00005); collagen alpha-2(I) chain (COL1A2; log₂FC = -2.97, p = 0.000003); protein S100-A16 (S100A16, log₂FC = -2.78, p = 0.001); nebulin (NEBL; log₂FC = -2.73, p = 0.0007); and mimecan (OGN; log₂FC = -2.47, p = 0.0001; Figure 3B). We examined the expression level of these proteins in the Human Protein Atlas (HPA) database²³ and found that majority of these proteins (EWSR1, TUBA1A, TIGAR, CENPV, COL1A2, S100A16, and NEBL) were up-regulated in ECs compared with normal endometrium tissue samples (Figure S2).

Previously, we have established that some proteins are differentially expressed in large uterine smooth muscle tumors compared with small tumors.²⁴ Here, we compared the proteome of macroscopic tumors (tumor volume >10 mm³) with microscopic tumors (<10 mm³; Table 1) to identify proteins that might be involved in promoting the growth of ECs. As expected, we found a significant number of proteins (1,835) that were commonly identified across the two tumor-size groups (Figure 3C). Our analysis also revealed a high number of differentially expressed proteins including 134 (6.8%) and 16 (0.8%) proteins exclusively found in macro- and microscopic tumors, respectively (Figure 3C). Volcano plot analysis revealed seven proteins that were significantly up-regulated in larger tumors, and these are EWSR1 (log₂FC = 2.43, p = 0.0003); enoyl-coenzyme A (CoA) hydratase mitochondrial (ECHS1; log₂FC = 1.35, p = 0.0004); D-3-phosphoglycerate dehydrogenase (PHGDH; log₂FC = 1.24, p = 0.000008); 14-3-3 protein epsilon (YWHAE; log₂FC = 1.16, p = 0.0005); hydroxyacyl-CoA dehydrogenase mitochondrial (HADH; log₂FC = 1.15, p = 0.0002); signal recognition particle subunit SRP68 (SRP68; log₂FC = 1.01, p = 0.00004), and caprin-1 (CAPRN1; log₂FC = 0.82, p = 0.00002) (Figure 3D). These seven proteins are more strongly expressed in EC than normal tissues (Figure S2), in agreement with our proteomic data. We also observed 32 proteins that were significantly more up-regulated in microscopic than larger tumors. Here, we have highlighted only the top five significant proteins, including hemoglobin subunit beta (HBB), band 3 anion transport protein (SLC4A1), fibrillin-1 (FBN1), transforming growth factor beta-1-induced transcript 1 protein (TGF-β111), and HBD (Figure 3D; see Table S2 for information on FC and p values).

Proteomic changes associated with myometrial invasion of cancer cells

The endometrium is surrounded by a thick layer of smooth muscle known as myometrium. Normally, endometrial cells are not

present in the myometrium. However, during the spread of EC, cancer cells invade the myometrium.^{10,21} The depth of invasion in the myometrium is indicative of the aggressive nature of EC. We categorized our patients based on the amount of myometrial invasion that was noted on histopathology reports of these patients by a pathologist. For myometrial invasion, we set a percentage score of greater than 10% to indicate that this group of patients has a higher depth of tumor infiltration into the myometrium. We detected 79 (4%) proteins only in highly invasive tumors and 22 (1.1%) proteins in less invasive tumors (<10% tumor invasion) (Figure 3E). For volcano plot analysis for myometrial invasion, we detected fifteen proteins that were statistically significant in their expression compared with the myometrial invasion less than 10% deep (Figure 3F). The top five candidate proteins are EWSR1 (logFC = 1.94, p = 0.0029); TIGAR (logFC = 1.72, p = 0.0034); Na(+)/H(+) exchange regulatory cofactor NHE-RF1 (SLC9A3R1; logFC = 1.67, p = 0.0003); DnaJ homolog subfamily B member 11 (DNAJB11; logFC = 1.43, p = 0.0011); and histone-binding protein RBBP4 (RBBP4; logFC = 1.38, p = 0.00007) (Figure 3F; Table S2). In addition, 48 proteins were down-regulated during deep myometrial invasion (>10%) including myosin-11 (MYH11; logFC = -2.88, p = 0.0011); NEBL (logFC = -2.46, p = 0.0001); COL1A2 (logFC = -2.40, p = 0.00001); OGN (logFC = -2.37, p = 0.001); and granulysin (GNLY; logFC = -2.24, p = 0.0005) (Figure 3F; Table S2). Overall, our comparative analysis of the proteome of ECs revealed protein signatures associated with tumor invasion.

Quantitation of proteins correlated with tumor grade

We next explored the proteomic profiles of different tumor grades in patients with EC. We first compared patients with grade 1 and 2 endometrioid carcinoma. Venn diagram analysis identified 1,860 proteins were commonly shared in grade 1 and 2 samples (Figure S3A). Of the total of 1,894 proteins identified in patients with EC with grade 2 tumors, only eight proteins were significantly up-regulated in grade 2 compared with grade 1 (Figure S3B). All of these proteins, EWSR1; marginal zone B- and B1-cell-specific protein (MZB1); interferon-induced GTP-binding protein Mx1 (MX1); sialic acid synthase (NANS); transmembrane emp24 domain-containing protein 9 (TMED9); tubulin polymerization-promoting protein family member 3 (TPPP3); heterogeneous nuclear ribonucleoprotein F (HNRNPF) and nucleolar and coiled-body phosphoprotein 1 (NOLC1), were found to be present at a greater abundance in the grade 2 samples (Figure S3B; Table S2; p < 0.01). On the other hand, 26 proteins were significantly down-regulated in grade 2 compared with grade 1 (Figure S3B; Table S2; p < 0.01). This includes proteins such as HBA1, COL1A2, SLC4A1, COL5A1, and fibrinogen alpha chain (FGA) (Figure S3B).

We also compared high-grade serous patients with grade 1 and 2 endometrioid carcinoma. 1,632 differentially expressed proteins between high-grade serous and grade 1 were screened out using the Venn diagram (Figure S3C). Analysis of patients with high-grade serous versus grade 1 EC revealed that 30 proteins were significantly up-regulated in high-grade serous and 18 were down-regulated (Figure S3C; Table S2). The top five significantly up- and down-regulated proteins are shown in Figure S3D. Comparative analysis of patients with grade 2

endometrioid carcinoma with high-grade serous patients revealed that 288 proteins were found exclusively in grade 2 patients and were not detected in high-grade samples (Figure S3E). From the set of 1,929 proteins, 6 proteins showed significantly elevated expression in the high-grade serous cohort compared with patients with grade 2 EC. These proteins are U1 small nuclear ribonucleoprotein C (SNRPC), COL1A1, COL1A2, translocation protein SEC63 homolog (SEC63), L-lactate dehydrogenase B chain (LDHB), and ABHD14B (Figure S3F; Table S2; $p < 0.01$). In contrast, the expression of 7 proteins was down-regulated, including lactotransferrin (LTF); glutathione S-transferase P (GSTP1); serine-tRNA ligase cytoplasmic (SARS1); sodium/potassium-transporting ATPase subunit beta-1 (ATP1B1); isoleucine-tRNA ligase cytoplasmic (IARS1); purine nucleoside phosphorylase (PNP); and 14-3-3 protein sigma (SFN), in high-grade serous patients (Figure S3F; Table S2; $p < 0.01$). Collectively, our results showed that tumors of different histological grades show diverse protein profiles at the proteomic level.

High EWSR1 expression is related to aggressive disease in older patients with EC

EWSR1 is an RNA/DNA-binding protein involved in multiple cellular processes, and its misregulation is observed in many human diseases.²⁵ Our proteomic analysis has revealed that high EWSR1 protein expression is present in large-size and invasive tumors, especially in postmenopausal patients (Figure 3 and S2). Next, we analyzed the status of EWSR1 in publicly available human tissue databases.^{26–28} Both single-cell RNA sequencing (scRNA-seq) and immunohistochemical analysis showed EWSR1 expression mainly in epithelial and stromal cells of the human endometrium (Figures S4A and S4B). In the cancer genome atlas for EC, high expression of EWSR1 at both mRNA and protein levels was observed in different subtypes of EC (Figure S4C). Tumors with altered EWSR1 expression were significantly different from unaltered EC samples and showed dysregulation in proteins involved in the DNA-repair pathway, such as TP53 and XRCC1 (Figures S4D–S4H). Immunohistochemical-based localization of EWSR1 in 70 tissue cores representing 35 different patients with EC revealed significantly higher expression of EWSR1 protein in older patients compared with their younger counterparts (Figures S4I and S4J). Overall, these findings suggest that higher EWSR1 expression marks a subset of endometrial tumors in aged women with highly aggressive pathology.

Analysis of patients with EC with alterations in DNA mismatch repair (MMR) proteins

EC is common in women with sporadic or hereditary (Lynch syndrome) defects in the MMR system.^{29,30} The MMR system is responsible for the repair of base substitutions together with deletions-insertions that might occur during DNA replication.^{29,30} The loss of MMR proteins often occurs in a pairwise manner, where the loss of MLH1 is accompanied by the absence of PMS2 and MLH2 loss is usually presented with the concurrent loss of MSH6.³¹ Patients with EC with the defective MMR system present with favorable clinical outcomes and show high sensitivity to adjuvant chemotherapy.^{29,30} Therefore, it is essential

that these patients are identified at the early stages and treated accordingly. We examined our patient cohort of 20 to see if we had some patients with a defective MMR system. We performed immunohistochemical localization of four proteins (MLH1, MLH2, MSH6, or PMS2) belonging to the MMR system and found that two patients with EC demonstrated loss of expression of MLH1/PMS2 proteins in epithelial cancer cells but not in the stroma (Figure 4A). We then compared patients with the defective versus intact MMR systems at the protein level and observed 75 (3.9%) and 80 (4.1%) exclusive proteins restricted to MLH⁻/PMS2⁻ and MLH⁺/PMS2⁺, respectively (Figure 4B). Volcano plot analysis further detected a total of 43 proteins, of which 40 were more abundant, while 3 were less abundant, in MLH^{+/ve}/PMS2^{+/ve} tumors compared with MLH^{-/ve}/PMS2^{-/ve} (Figure 4C). Of the 40 more abundant proteins, HBA1, COL1A2, transcriptional coactivator YAP1 (YAP1), parathymosin (PTMS), and cell division cycle and apoptosis regulator protein 1 (CCAR) were found to be the most significant in MLH1⁺/PMS2⁺ tumors (Figure 4C). Moreover, we found three proteins, namely Crk-like protein (CRKL), dolichyl-diphosphooligosaccharide-protein glycosyltransferase subunit DAD1 (DAD1), and aspartyl/asparaginyl beta-hydroxylase (ASPH), that were down-regulated in MLH⁺/PMS2⁺ tumors (Figure 4C). These data suggest that CRKL, DAD1, and ASPH expression could serve as a prognostic biomarker in differentiating between MMR intact and deficient tumors in patients with EC.

Common signaling proteins across all the patients with cancer

Despite EC heterogeneity, all patients with EC are treated with a relatively similar treatment regime.²¹ Therefore, we were interested in identifying common pathways or protein networks that are present in the majority of patients with EC. To do this, we extracted the list of common EC proteins identified from individual patients and compared them with their corresponding adjacent normal endometrium (ANE) tissues. We repeated this analysis for the other patients with EC. Only those EC proteins that were not found in the healthy control were further included in the Venn diagrams and then compared across patients with EC based on their tumor classification (grades I and II, respectively; Table 1). Nested Venn diagram of these EC grade I proteins that were present in tumors but absent in ANE led to the detection of 1,637 proteins. A calcium-binding protein, namely grancalcin (GCA), was one that was commonly detected across six out of eight patients with grade I EC (Figure 5A). In contrast to grade I patients, five proteins were frequently detected from five out of six patients with grade II EC, and they are mRNA turnover protein 4 homolog (MRTO4); minor histocompatibility antigen H13 (HM13); proteasome subunit beta type-9 (PSMB9); transmembrane emp24 domain-containing protein 7 (TMED7); and glutamine-fructose-6-phosphate aminotransferase 1 (GFPT1) (Figure 5B). All of these proteins (GCA, MRTO4, HM13, PSMB9, TMED7, and GFPT1) may be potential markers for distinguishing histological grade in EC.

To discern the most prevalent and significantly perturbed canonical pathways in 20 patients with EC, we imported our datasets of the common protein profiles identified from different

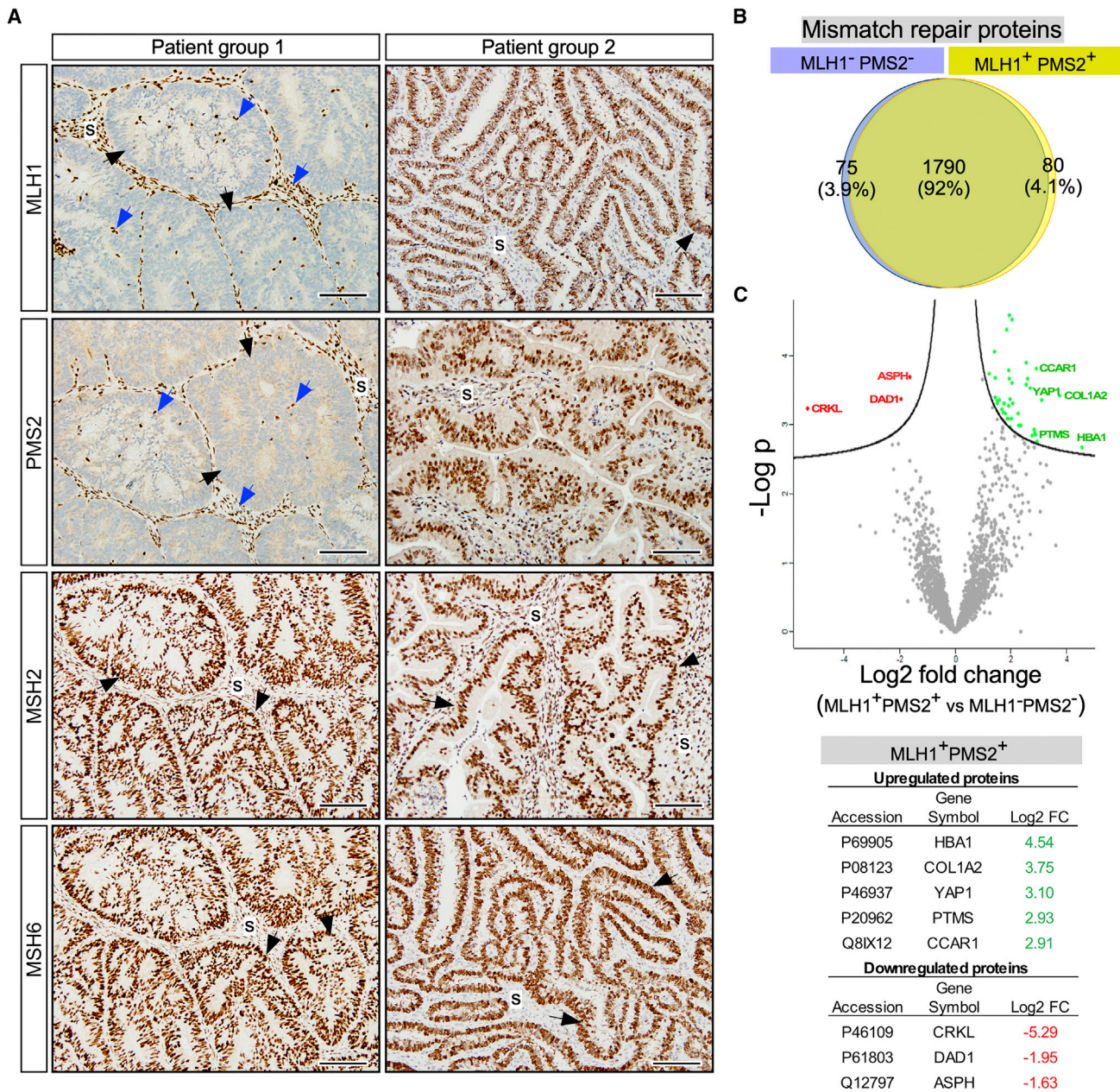


Figure 4. Analysis of endometrial cancers with the defects in the DNA mismatch repair (MMR) system

(A) Group 1 of patients with EC showed loss of MLH1 and PMS2 proteins compared with patient group 2 (MLH1⁺/PMS2⁺). Epithelial cells are marked by black arrows and the stromal cells by blue arrows. Scale bars, 100 μ m.

(B) Venn diagram depicts overlapped and unique quantifiable proteins identified in patients with EC harboring MMR (MLH1/PMS2 negative versus MLH1/PMS2 positive).

(C) Volcano plots show the difference in fold change (x axis) and the significance of the difference (y axis) in patients with EC between positive and negative MLH1/PMS2. Proteins that pass a p value threshold for either up- or down-regulated expression are highlighted in green and red, respectively. The top significant up- and down-regulated proteins are shown in the table.

locations within an EC tissue into the ingenuity pathway analysis (IPA) database. We then extracted the top ten pathways found in a single patient and mapped them across the other patients with EC (Figure 5C). The functional pathways or networks with the highest confidence scores were then determined by right-tailed

Fisher's exact test. IPA analysis across all patients with EC showed significant association with eukaryotic initiation factor 2 (eIF2) signaling. It is worth noting that eIF2 is essential for regulating protein synthesis at the level of translation initiation.³² Misregulation of protein synthesis linked to the high expression of

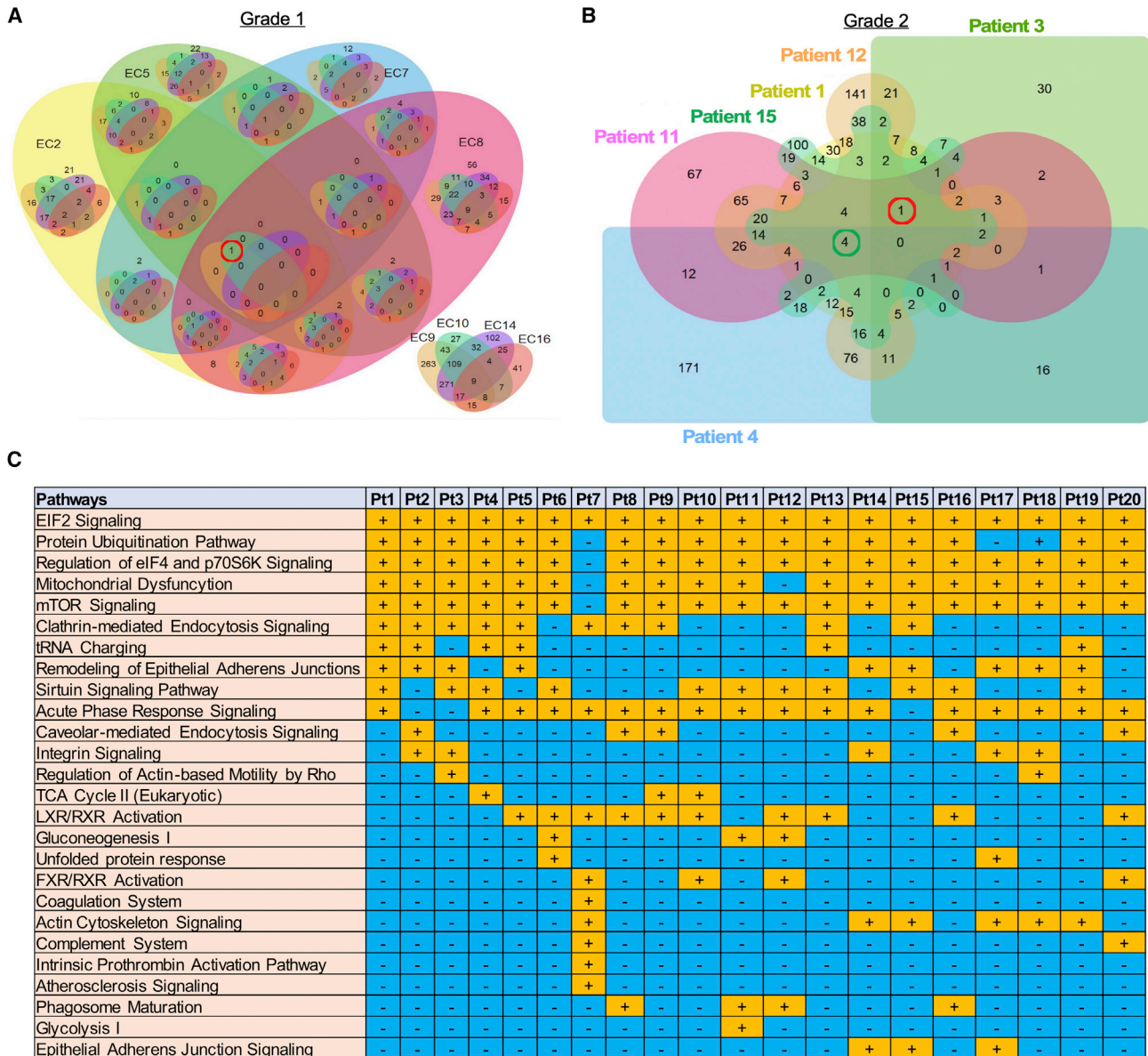


Figure 5. Assessment of common proteins across different patients

Nestlé and Edward's Venn diagrams visualize the number of shared and differentially expressed EC proteins that are not found in the healthy controls in 8 patients with grade 1 EC and 6 patients with grade 2 EC, respectively.

(A) GCA (circled in red) was one of the frequently detected proteins from six out of eight patients with grade 1 EC.

(B) MRT04, HM13, PSMB9, TMED7 (circled in green), and GFPT1 (circled in red) were commonly identified in five out of six patients with grade 2 EC.

(C) Ingenuity pathway analysis (IPA) highlights the common top 10 canonical pathways significantly altered and detected across 20 patients with EC.

eIF2 α has been reported in many cancers (Hodgkin's lymphoma, lung, gastrointestinal, and melanoma),^{33,34} and this protein may play a similar role during EC tumor progression. IPA analysis also identified the involvement of two other signaling networks in 19 patients with EC, and they are regulation of eIF4 and ribosomal protein S6 kinase beta-1 (p70S6K) signaling and mTOR signaling. Our findings suggested that targeting of these common signaling pathways found in the majority of patients with EC may hold promise to overcoming EC. The top 10 most signif-

icant canonical pathways in the respective 20 patients with EC are listed in [Figure S5](#).

Patient-derived EC organoids represent the heterogeneity of the native tumor

Patient-derived organoids (PDOs) have now become a preferred method of modeling cancer because they retain the cellular and molecular characteristic of the patient tumor and mimic a patient's clinical responses to treatments.³⁵ PDOs are typically

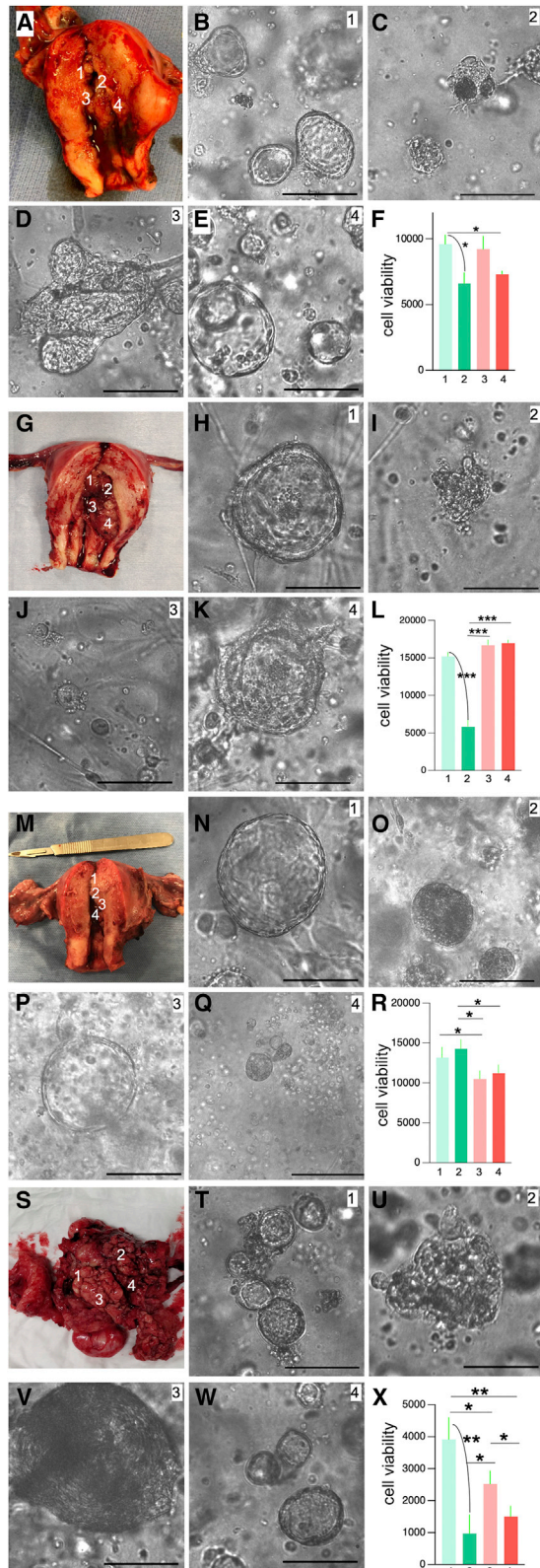


Figure 6. Patient-derived endometrial cancer organoids capture heterogeneity of the primary tumor

(A–X) Gross images of patients’ uteri and organoids derived from the different regions of patient tumors (n = 16 biopsies from 4 patients with EC). Bar charts represent the cell viability of organoids derived from different sites of EC within the same patient at 10 days of culture. Statistical analysis was performed using an unpaired t test. Data are presented as mean ± SEM. Significant differences are indicated by *p < 0.05, **p < 0.01, and ***p < 0.001.

developed from a single tiny biopsy representing the patient tumor.³⁶ To model EC heterogeneity, we developed organoids from four different biopsies representing four different tumor regions from a single patient (Figure 6). Fresh tumor biopsies were collected from tumor mass present in the uterus and immediately processed to grow organoids. In total, organoids were developed from 16 EC biopsies collected from four patients. Grossly, EC organoids derived from different regions of a patient tumor appeared different in shape and size (Figure 6). These morphology differences in PDOs were present irrespective of the size of the native tumor from where these biopsies were obtained (Figure 6). We analyzed the growth of PDOs after 10 days of culture using a standard cell viability assay³⁷ and observed significant differences in the growth of EC organoids representing different regions of the same tumor (Figure 6). Collectively, these results confirmed that the proteomic differences we have observed within the same tumor of a patient also translate to differences in the growth rate of tumor cells.

DISCUSSION

EC remains the most common gynecological cancer in developed countries.^{38,39} Despite efforts into finding new prevention, diagnostic, and therapeutic targets, the mortality and morbidity rates associated with EC continue to rise.⁴⁰ The current treatment strategies for ECs are limited to surgery and adjuvant therapies. Therefore, an in-depth understanding of the molecular mechanisms underlying this heterogeneous disease, particularly at the protein level, will allow for the identification of new treatment options for EC.

One of the main challenges for the characterization of biomarkers and treatment selection for EC is intra-tumor heterogeneity. This phenomenon refers to the co-existence of distinct subpopulations of cancer cells with different genetic and phenotypic profiles within a given primary tumor and between a given primary tumor and its metastases.^{41,42} The diversity of these cancer cell populations can be attributed to activation of signaling or metabolic pathways, tumorigenicity, metastasis, migration, and escape from anti-tumor immunity.^{43,44} In this study, we explored endometrial heterogeneity using MS to define the proteome of EC and identify the unique expression of proteins found in the different locations of EC within individual patients. Our research data showed that tissue samples taken from several sites of EC from the same patient possess diverse proteomic profiles. Genomic analysis of benign human endometrium has depicted that the genomic architecture of epithelial cells in the uterus is heterogeneous,¹⁷ which is consistent with our observations at the proteomic level in EC. Our data show that there are proteins unique to each sample, ranging from 86 to 327 exclusive proteins per patient. This demonstrates that unique groups of proteins only exist

in one EC location but are not found in other locations within the same tumor. Furthermore, we assessed all of these EC proteins in relation to their patient menopausal conditions, tumor size and grade, and the depth of myometrial invasion. From this analysis, EWSR1, a multifunctional protein, was one of the most significantly up-regulated candidates in the postmenopausal patient group. EWSR1, also known to be involved in the development of Ewing sarcoma,⁴⁵ is a nuclear protein encoding 656 amino acids that traffic between the nucleus and cytoplasm.^{46,47} EWSR1 belongs to the TET family of RNA-binding proteins, and it is implicated in transcriptional regulation and RNA processing.^{48–50} EWSR1 mainly contains an N-terminal transcription activation domain and a C-terminal nucleic acid binding domain.⁵¹ EWSR1 is known to be involved in a diverse range of human solid tumors besides Ewing sarcoma, including primitive neuroectodermal tumors,⁵² desmoplastic small round cell tumor,⁵³ angiomatoid fibrous histiocytoma,⁵⁴ and myoepithelial tumors of the skin, soft tissue, and bone.⁵⁵ Our data have identified the expression levels of EWSR1 is high in patients with EC during postmenopausal stages, as well as up-regulated in macroscopic and more invasive tumors. In this regard, the overexpression of EWSR1 in EC represents the most valuable candidate for further functional and clinical investigations. The exact mechanisms underlying the invasive properties of EWSR1 in EC are still largely uncertain, but translocation of EWSR1 and its binding partner is known to promote tumorigenesis.^{56,57} It is, therefore, possible that the altered interactions between EWSR1 and its various partner encoding transcriptional regulators are involved in the process of endometrial carcinogenesis.

Compared with postmenopausal patients with EC, TMSB4X protein has been found to be highly overexpressed in premenopausal patients with EC. TMSB4X is a small 5 kDa protein comprising 44 amino acids that act as a regulator for actin polymerization.⁵⁸ Enhanced levels of TMSB4X is detected in various cancers linked to pancreatic,⁵⁹ colorectal,⁶⁰ and gastric.⁶¹ A previous study has reported that TMSB4X has been implicated in human tumor progression, metastasis, and cell motility.⁶² Although no study has explored the role of TMSB4X in EC, our proteomic screening on the TMSB4 overexpression sheds light on an unexpected pathway that drives EC metastasis. TMSB4X could be served as a potential therapeutic target, particularly in premenopausal patients with EC.

A comparison of expression levels between macro- versus microscopic revealed that HBB, a globin protein, was one of the highest up-regulated proteins in microscopic tumors. It is possible that these tumors grow as they progress, and these microscopic tumors could indicate early stages of EC. Therefore, because of elevated levels of HBB in microscopic tumors, this HBB protein may have the potential as a drug target to prevent the progression of EC. We also examined the protein expression of myometrial invasion in these patients with EC. Deep myometrial infiltration is associated with increased undifferentiated tumors, invasion of lymph-vascular, and reduced global survival.⁶³ Our proteomic analysis pointed to EWSR1 and MYH11 up-regulation during myometrial infiltration >10% and <10%, respectively. MYH11 encodes the smooth muscle myosin heavy chain, essential for regulating smooth muscle contraction.⁶⁴ Intense MYH11 expression is strongly associated with endoplasmic reticulum (ER) stress

response caused by the accumulation of misfolded proteins and induces autophagy in human diseases, including neurodegenerative disorders and cancer.^{64–66} We can only speculate that the MYH11 protein may contribute similar drive during myometrial infiltration processes in EC, but further work will be needed to determine the exact mechanisms. EWSR1 and MYH11 could potentially serve as markers to differentiate the early and late stages of invasion in EC.

In addition, we also investigated patients with EC with potential Lynch syndrome-associated DNA MMR protein expression. Lynch syndrome, also known as hereditary non-polyposis colorectal cancer (HNPCC), is an autosomal dominant disorder that is responsible for the majority of inherited EC cases.⁶⁷ This condition is mainly caused by germ-line mutations in the DNA MMR genes *MLH1*, *MSH2*, *MSH6*, or *PMS2*.⁶⁸ Alterations in the MMR genes are also known to occur in sporadic ECs.^{29,30} We detected the loss of MLH1 and PMS2 proteins in the epithelial cancer cells of two patients with EC. The loss of MLH1 and PMS2 has been recently reported during the early histological changes associated with the development of endometrial neoplasia, and they have been proposed as markers for distinguishing neoplastic lesions from benign endometrium.⁶⁹ We then compared the two patients with EC (MLH1^{-ve}/PMS2^{-ve}) with the selected five patients with EC (MLH1^{+ve}/PMS2^{+ve}) at the protein level. The present study explores differential protein expression of Lynch syndrome-associated DNA MMR between the two groups of patients with EC (MLH1^{-ve}/PMS2^{-ve} versus MLH1^{+ve}/PMS2^{+ve}). Interestingly, comparative analysis of these two groups revealed that CRK-like proto-oncogene, adaptor protein (CRKL), defender against cell death 1 (DAD1), and Aspartate beta-hydroxylase (ASPH) were significantly down-regulated in tumors positive for MLH1/PMS2 compared with MLH1^{-ve}/PMS2^{-ve}. CRKL is a signaling adapter protein that plays a vital role in cell proliferation and migration.⁷⁰ Overexpression of CRKL has been associated with various cancer types, including breast cancer,⁷¹ lung cancer,⁷² and pancreatic cancer.⁷³ DAD1 is a regulatory protein that inhibits apoptotic cell death and is a downstream target of the nuclear factor κ B (NF- κ B) survival pathway.⁷⁴ Elevated levels of NF- κ B and DAD1 have been linked with perineural invasion in prostate cancer.⁷⁵ ASPH is a type II transmembrane protein located in the endoplasmic reticulum, where its function is required for the malignant transformation of cells and promotes tumor progression.⁷⁶ These three proteins represent potential markers for differentiating ECs associated with Lynch syndrome and/or defective MMR systems. The patient number with MLH1^{-ve}/PMS2^{-ve} ECs was limiting in this study, and therefore, further studies using a larger cohort of these patients are required to validate these results.

Together, our work has defined EC heterogeneity using quantitative proteomics and PDOs. Our work suggests that a single biopsy-based protocol might not be appropriate for conducting clinical trials with targeted therapies in ECs and, possibly, in other solid cancers. Importantly, our datasets will be useful in further investigations into the mechanisms of endometrial heterogeneity.

LIMITATIONS OF THE STUDY

The study analyzed 63 biopsies from 20 patients using LC-MS and developed organoids using 16 biopsies collected from 4

patients. Our spectral library for SWATH-MS consists of 2,175 proteins, which is on the lower side of the coverage predicted to be achieved using data-independent acquisition (DIA)/SWATH methods. We believe that the highly complex nature of primary tumors and applying a strict threshold of 99% confidence (<1% FDR) to select peptides might have affected the total number of proteins detected in this study. A follow-up study using a larger cohort of patients is now required to validate some of the key observations of the present study. Our study identified prognostic biomarkers differentiating between MMR-intact (MLH1^{+ve}/PMS2^{+ve}) and MMR-deficient (MLH1^{-ve}/PMS2^{-ve}) tumors. However, our sample size was limited for patients with Lynch syndrome (MLH1^{-ve}/PMS2^{-ve}). Therefore, a follow-up study with a larger cohort of patients with Lynch syndrome is needed to confirm these prognostic markers.

STAR★METHODS

Detailed methods are provided in the online version of this paper and include the following:

- **KEY RESOURCES TABLE**
- **RESOURCE AVAILABILITY**
 - Lead Contact
 - Materials availability
 - Data and code availability
- **EXPERIMENTAL MODEL AND SUBJECT DETAILS**
- **METHOD DETAILS**
 - Protein extraction and digestion
 - Library generation for SWATH analysis and LC-MS/MS acquisition
 - SWATH analysis and data processing
 - Ingenuity pathway analysis (IPA)
 - Mismatch repair (MMR) protein detection
 - Patient-derived endometrial cancer organoids
- **QUANTIFICATION AND STATISTICAL ANALYSIS**

SUPPLEMENTAL INFORMATION

Supplemental information can be found online at <https://doi.org/10.1016/j.crm.2022.100738>.

ACKNOWLEDGMENTS

Work in the Tanwar lab was in part supported by funding from National Health and Medical Research Council, Cancer Australia, Ovarian Cancer Research Foundation, and The Dorothy Jean Cunningham Endometrial Cancer Research Bequest. We thank Dr. Manish Kumar and Varshini Venkata for technical assistance, Dr. Jim Scurry (pathologist) for histopathological inputs, and Nathan Smith at the University ABRF facility for help with LC-MS/MS. Some illustrations were created using BioRender software.

AUTHOR CONTRIBUTIONS

P.S.T. designed research; M.F.B.J., Y.-A.K., A.G., S.M.S., and J.K.N. performed research; Y.I., R.O., M.A.B., P.N., and K.J. contributed new reagents; M.F.B.J. and P.S.T. analyzed data and wrote the paper.

DECLARATION OF INTERESTS

The author reports no conflicts of interest in this work.

INCLUSION AND DIVERSITY

One or more of the authors of this paper self-identifies as an underrepresented ethnic minority in science. While citing references scientifically relevant for this work, we also actively worked to promote gender balance in our reference list. The author list of this paper includes contributors from the location where the research was conducted who participated in the data collection, design, analysis, and/or interpretation of the work.

Received: November 2, 2021

Revised: June 1, 2022

Accepted: August 18, 2022

Published: September 13, 2022

REFERENCES

1. Lu, K.H., and Broaddus, R.R. (2020). Endometrial cancer. *N. Engl. J. Med.* 383, 2053–2064. <https://doi.org/10.1056/NEJMra1514010>.
2. Llauradó, M., Ruiz, A., Majem, B., Ertekin, T., Colás, E., Pedrola, N., Devis, L., Rigau, M., Sequeiros, T., Montes, M., et al. (2012). Molecular bases of endometrial cancer: new roles for new actors in the diagnosis and the therapy of the disease. *Mol. Cell. Endocrinol.* 358, 244–255. <https://doi.org/10.1016/j.mce.2011.10.003>.
3. Siegel, R.L., Miller, K.D., Fuchs, H.E., and Jemal, A. (2021). Cancer statistics, 2021. *CA Cancer J. Clin.* 71, 7–33. <https://doi.org/10.3322/caac.21654>.
4. Morice, P., Leary, A., Creutzberg, C., Abu-Rustum, N., and Darai, E. (2016). Endometrial cancer. *Lancet* 387, 1094–1108. [https://doi.org/10.1016/s0140-6736\(15\)00130-0](https://doi.org/10.1016/s0140-6736(15)00130-0).
5. Colombo, N., Preti, E., Landoni, F., Carinelli, S., Colombo, A., Marini, C., and Sessa, C.; ESMO Guidelines Working Group (2013). Endometrial cancer: ESMO Clinical Practice Guidelines for diagnosis, treatment and follow-up. *Ann. Oncol.* 24, vi33–38. <https://doi.org/10.1093/annonc/mdt353>.
6. Wright, J.D., Barrena Medel, N.I., Sehouli, J., Fujiwara, K., and Herzog, T.J. (2012). Contemporary management of endometrial cancer. *Lancet* 379, 1352–1360. [https://doi.org/10.1016/s0140-6736\(12\)60442-5](https://doi.org/10.1016/s0140-6736(12)60442-5).
7. Lewin, S.N., Herzog, T.J., Barrena Medel, N.I., Deutsch, I., Burke, W.M., Sun, X., and Wright, J.D. (2010). Comparative performance of the 2009 international Federation of gynecology and obstetrics' staging system for uterine corpus cancer. *Obstet. Gynecol.* 116, 1141–1149. <https://doi.org/10.1097/AOG.0b013e3181f39849>.
8. Tejerizo-García, A., Jiménez-López, J.S., Muñoz-González, J.L., Bartolomé-Sotillos, S., Marqueta-Marqués, L., López-González, G., and Gómez, J.F.P.R. (2013). Overall survival and disease-free survival in endometrial cancer: prognostic factors in 276 patients. *OncoTargets Ther.* 9, 1305–1313. <https://doi.org/10.2147/ott.s51532>.
9. Cancer Genome Atlas Research Network; Kandoth, C., Schultz, N., Cherniack, A.D., Akbani, R., Liu, Y., Shen, H., Robertson, A.G., Pashtan, I., Shen, R., et al. (2013). Integrated genomic characterization of endometrial carcinoma. *Nature* 497, 67–73. <https://doi.org/10.1038/nature12113>.
10. Di Cristofano, A., and Ellenson, L.H. (2007). Endometrial carcinoma. *Annu. Rev. Pathol.* 2, 57–85. <https://doi.org/10.1146/annurev.pathol.2.010506.091905>.
11. Daikoku, T., Hirota, Y., Tranguch, S., Joshi, A.R., DeMayo, F.J., Lydon, J.P., Ellenson, L.H., and Dey, S.K. (2008). Conditional loss of uterine Pten unfaithfully and rapidly induces endometrial cancer in mice. *Cancer Res.* 68, 5619–5627. <https://doi.org/10.1158/0008-5472.CAN-08-1274>.
12. Weigelt, B., Warne, P.H., Lambros, M.B., Reis-Filho, J.S., and Downward, J. (2013). PI3K pathway dependencies in endometrioid endometrial cancer cell lines. *Clin. Cancer Res.* 19, 3533–3544. <https://doi.org/10.1158/1078-0432.CCR-12-3815>.
13. Mackay, H.J., Eisenhauer, E.A., Kamel-Reid, S., Tsao, M., Clarke, B., Karakasis, K., Werner, H.M.J., Trovik, J., Akslen, L.A., Salvesen, H.B., et al.

- (2014). Molecular determinants of outcome with mammalian target of rapamycin inhibition in endometrial cancer. *Cancer* 120, 603–610. <https://doi.org/10.1002/cncr.28414>.
14. Lheureux, S., and Oza, A.M. (2016). Endometrial cancer-targeted therapies myth or reality? Review of current targeted treatments. *Eur. J. Cancer* 59, 99–108. <https://doi.org/10.1016/j.ejca.2016.02.016>.
 15. Hussein, N., and Hussein, H.D. (2014). mTOR inhibitors and their clinical application in cervical, endometrial and ovarian cancers: a critical review. *Gynecol. Oncol.* 133, 375–381. <https://doi.org/10.1016/j.ygyno.2014.02.017>.
 16. Mutter, G.L., Monte, N.M., Neuber, D., Ferenczy, A., and Eng, C. (2014). Emergence, involution, and progression to carcinoma of mutant clones in normal endometrial tissues. *Cancer Res.* 74, 2796–2802. <https://doi.org/10.1158/0008-5472.CAN-14-0108>.
 17. Suda, K., Nakaoka, H., Yoshihara, K., Ishiguro, T., Tamura, R., Mori, Y., Yamawaki, K., Adachi, S., Takahashi, T., Kase, H., et al. (2018). Clonal expansion and diversification of cancer-associated mutations in endometriosis and normal endometrium. *Cell Rep.* 24, 1777–1789. <https://doi.org/10.1016/j.celrep.2018.07.037>.
 18. Supernat, A., Lapińska-Szumczyk, S., Majewska, H., Gulczyński, J., Biernat, W., Wydra, D., and Zaczek, A.J. (2014). Tumor heterogeneity at protein level as an independent prognostic factor in endometrial cancer. *Transl. Oncol.* 7, 613–619. <https://doi.org/10.1016/j.tranon.2014.06.001>.
 19. Ludwig, C., Gillet, L., Rosenberger, G., Amon, S., Collins, B.C., and Aebersold, R. (2018). Data-independent acquisition-based SWATH-MS for quantitative proteomics: a tutorial. *Mol. Syst. Biol.* 14, e8126. <https://doi.org/10.15252/msb.20178126>.
 20. Hoffman, K., Nekhlyudov, L., and Deligdisch, L. (1995). Endometrial carcinoma in elderly women. *Gynecol. Oncol.* 58, 198–201. <https://doi.org/10.1006/gy.1995.1210>.
 21. Sahoo, S.S., Zhang, X.D., Hondermarck, H., and Tanwar, P.S. (2018). The emerging role of the microenvironment in endometrial cancer. *Cancers* 10, E408. <https://doi.org/10.3390/cancers10110408>.
 22. Hall, J.E. (2015). Endocrinology of the menopause. *Endocrinol. Metab. Clin. North Am.* 44, 485–496. <https://doi.org/10.1016/j.ecl.2015.05.010>.
 23. Asplund, A., Edqvist, P.H.D., Schwenk, J.M., and Pontén, F. (2012). Antibodies for profiling the human proteome—The Human Protein Atlas as a resource for cancer research. *Proteomics* 12, 2067–2077. <https://doi.org/10.1002/pmic.201100504>.
 24. Jamaluddin, M.F.B., Ko, Y.A., Kumar, M., Brown, Y., Bajwa, P., Nagendra, P.B., Skerrett-Byrne, D.A., Hondermarck, H., Baker, M.A., Dun, M.D., et al. (2018). Proteomic profiling of human uterine fibroids reveals upregulation of the extracellular matrix protein periostin. *Endocrinology* 159, 1106–1118. <https://doi.org/10.1210/en.2017-03018>.
 25. Lee, J., Nguyen, P.T., Shim, H.S., Hyeon, S.J., Im, H., Choi, M.H., Chung, S., Kowall, N.W., Lee, S.B., and Ryu, H. (2019). EWSR1, a multifunctional protein, regulates cellular function and aging via genetic and epigenetic pathways. *Biochim. Biophys. Acta Mol. Basis Dis.* 1865, 1938–1945. <https://doi.org/10.1016/j.bbdis.2018.10.042>.
 26. Gao, J., Aksoy, B.A., Dogrusoz, U., Dresdner, G., Gross, B., Sumer, S.O., Sun, Y., Jacobsen, A., Sinha, R., Larsson, E., et al. (2013). Integrative analysis of complex cancer genomics and clinical profiles using the cBioPortal. *Sci. Signal.* 6, pii. <https://doi.org/10.1126/scisignal.2004088>.
 27. Karlsson, M., Zhang, C., Méar, L., Zhong, W., Digre, A., Katona, B., Sjöstedt, E., Butler, L., Odeberg, J., Dusart, P., et al. (2021). A single-cell type transcriptomics map of human tissues. *Sci. Adv.* 7, eabh2169. <https://doi.org/10.1126/sciadv.abh2169>.
 28. Uhlén, M., Fagerberg, L., Hallström, B.M., Lindskog, C., Oksvold, P., Mardinoglu, A., Sivertsson, Å., Kampf, C., Sjöstedt, E., Asplund, A., et al. (2015). Proteomics. Tissue-based map of the human proteome. *Science* 347, 1260419. <https://doi.org/10.1126/science.1260419>.
 29. Shikama, A., Minaguchi, T., Matsumoto, K., Akiyama-Abe, A., Nakamura, Y., Michikami, H., Nakao, S., Sakurai, M., Ochi, H., Onuki, M., et al. (2016). Clinicopathologic implications of DNA mismatch repair status in endometrial carcinomas. *Gynecol. Oncol.* 140, 226–233. <https://doi.org/10.1016/j.ygyno.2015.11.032>.
 30. Black, D., Soslow, R.A., Levine, D.A., Tornos, C., Chen, S.C., Hummer, A.J., Bogomolny, F., Olvera, N., Barakat, R.R., and Boyd, J. (2006). Clinicopathologic significance of defective DNA mismatch repair in endometrial carcinoma. *J. Clin. Oncol.* 24, 1745–1753. <https://doi.org/10.1200/JCO.2005.04.1574>.
 31. Boland, C.R., Koi, M., Chang, D.K., and Carethers, J.M. (2008). The biochemical basis of microsatellite instability and abnormal immunohistochemistry and clinical behavior in Lynch syndrome: from bench to bedside. *Fam. Cancer* 7, 41–52. <https://doi.org/10.1007/s10689-007-9145-9>.
 32. Kimball, S.R. (1999). Eukaryotic initiation factor eIF2. *Int. J. Biochem. Cell Biol.* 31, 25–29.
 33. Spilka, R., Ernst, C., Mehta, A.K., and Haybaeck, J. (2013). Eukaryotic translation initiation factors in cancer development and progression. *Cancer Lett.* 340, 9–21. <https://doi.org/10.1016/j.canlet.2013.06.019>.
 34. Zheng, Q., Ye, J., and Cao, J. (2014). Translational regulator eIF2alpha in tumor. *Tumour Biol.* 35, 6255–6264. <https://doi.org/10.1007/s13277-014-1789-0>.
 35. Veninga, V., and Voest, E.E. (2021). Tumor organoids: opportunities and challenges to guide precision medicine. *Cancer Cell* 39, 1190–1201. <https://doi.org/10.1016/j.ccell.2021.07.020>.
 36. Boretto, M., Maenhoudt, N., Luo, X., Hennes, A., Boeckx, B., Bui, B., Heremans, R., Perneel, L., Kobayashi, H., Van Zundert, I., et al. (2019). Patient-derived organoids from endometrial disease capture clinical heterogeneity and are amenable to drug screening. *Nat. Cell Biol.* 21, 1041–1051. <https://doi.org/10.1038/s41556-019-0360-z>.
 37. Seidlitz, T., Merker, S.R., Rothe, A., Zakrzewski, F., von Neubeck, C., Grützmann, K., Sommer, U., Schweitzer, C., Schölich, S., Uhlemann, H., et al. (2019). Human gastric cancer modelling using organoids. *Gut* 68, 207–217. <https://doi.org/10.1136/gutjnl-2017-314549>.
 38. Siegel, R.L., Miller, K.D., and Jemal, A. (2018). Cancer statistics, 2018. *CA Cancer J. Clin.* 68, 7–30. <https://doi.org/10.3322/caac.21442>.
 39. Amant, F., Moerman, P., Neven, P., Timmerman, D., Van Limbergen, E., and Vergote, I. (2005). Endometrial cancer. *Lancet* 366, 491–505. [https://doi.org/10.1016/s0140-6736\(05\)67063-8](https://doi.org/10.1016/s0140-6736(05)67063-8).
 40. Lindemann, K., Eskild, A., Vatten, L.J., and Bray, F. (2010). Endometrial cancer incidence trends in Norway during 1953–2007 and predictions for 2008–2027. *Int. J. Cancer* 127, 2661–2668. <https://doi.org/10.1002/ijc.25267>.
 41. Marusyk, A., Almendro, V., and Polyak, K. (2012). Intra-tumour heterogeneity: a looking glass for cancer? *Nat. Rev. Cancer* 12, 323–334. <https://doi.org/10.1038/nrc3261>.
 42. Marusyk, A., and Polyak, K. (2010). Tumor heterogeneity: causes and consequences. *Biochim. Biophys. Acta* 1805, 105–117. <https://doi.org/10.1016/j.bbcan.2009.11.002>.
 43. Michor, F., and Polyak, K. (2010). The origins and implications of intratumor heterogeneity. *Cancer Prev. Res.* 3, 1361–1364. <https://doi.org/10.1158/1940-6207.capr-10-0234>.
 44. Andrechek, E.R., and Nevins, J.R. (2010). Mouse models of cancers: opportunities to address heterogeneity of human cancer and evaluate therapeutic strategies. *J. Mol. Med.* 88, 1095–1100. <https://doi.org/10.1007/s00109-010-0644-z>.
 45. Ludwig, J.A. (2008). Ewing sarcoma: historical perspectives, current state-of-the-art, and opportunities for targeted therapy in the future. *Curr. Opin. Oncol.* 20, 412–418. <https://doi.org/10.1097/CCO.0b013e328303ba1d>.
 46. Fisher, C. (2014). The diversity of soft tissue tumours with EWSR1 gene rearrangements: a review. *Histopathology* 64, 134–150. <https://doi.org/10.1111/his.12269>.
 47. Leemann-Zakaryan, R.P., Pahlich, S., Grossenbacher, D., and Gehring, H. (2011). Tyrosine phosphorylation in the C-terminal nuclear localization and

- retention signal (C-NLS) of the EWS protein. *Sarcoma* 2011, 218483. <https://doi.org/10.1155/2011/218483>.
48. Law, W.J., Cann, K.L., and Hicks, G.G. (2006). TLS, EWS and TAF15: a model for transcriptional integration of gene expression. *Brief. Funct. Genomic. Proteomic.* 5, 8–14. <https://doi.org/10.1093/bfgp/ell015>.
 49. Tan, A.Y., and Manley, J.L. (2009). The TET family of proteins: functions and roles in disease. *J. Mol. Cell Biol.* 1, 82–92. <https://doi.org/10.1093/jmcb/mjp025>.
 50. Paronetto, M.P., Miñana, B., and Valcárcel, J. (2011). The Ewing sarcoma protein regulates DNA damage-induced alternative splicing. *Mol. Cell* 43, 353–368. <https://doi.org/10.1016/j.molcel.2011.05.035>.
 51. Zakaryan, R.P., and Gehring, H. (2006). Identification and characterization of the nuclear localization/retention signal in the EWS proto-oncoprotein. *J. Mol. Biol.* 363, 27–38. <https://doi.org/10.1016/j.jmb.2006.08.018>.
 52. Arvand, A., and Denny, C.T. (2001). Biology of EWS/ETS fusions in Ewing's family tumors. *Oncogene* 20, 5747–5754. <https://doi.org/10.1038/sj.onc.1204598>.
 53. Gerald, W.L., Rosai, J., and Ladanyi, M. (1995). Characterization of the genomic breakpoint and chimeric transcripts in the EWS-WT1 gene fusion of desmoplastic small round cell tumor. *Proc. Natl. Acad. Sci. USA* 92, 1028–1032.
 54. Rossi, S., Szuhai, K., Ijszenga, M., Tanke, H.J., Zanatta, L., Sciort, R., Fletcher, C.D.M., Dei Tos, A.P., and Hogendoorn, P.C.W. (2007). EWSR1-CREB1 and EWSR1-ATF1 fusion genes in angiomatoid fibrous histiocytoma. *Clin. Cancer Res.* 13, 7322–7328. <https://doi.org/10.1158/1078-0432.ccr-07-1744>.
 55. Antonescu, C.R., Zhang, L., Chang, N.E., Pawel, B.R., Travis, W., Katabi, N., Edelman, M., Rosenberg, A.E., Nielsen, G.P., Dal Cin, P., and Fletcher, C.D.M. (2010). EWSR1-POU5F1 fusion in soft tissue myoepithelial tumors. A molecular analysis of sixty-six cases, including soft tissue, bone, and visceral lesions, showing common involvement of the EWSR1 gene. *Genes Chromosomes Cancer* 49, 1114–1124. <https://doi.org/10.1002/gcc.20819>.
 56. Zucman, J., Delattre, O., Desmazes, C., Epstein, A.L., Stenman, G., Spleman, F., Fletchers, C.D., Aurias, A., and Thomas, G. (1993). EWS and ATF-1 gene fusion induced by t(12;22) translocation in malignant melanoma of soft parts. *Nat. Genet.* 4, 341–345. <https://doi.org/10.1038/ng0893-341>.
 57. Bailly, R.A., Bosselut, R., Zucman, J., Cormier, F., Delattre, O., Roussel, M., Thomas, G., and Ghysdael, J. (1994). DNA-binding and transcriptional activation properties of the EWS-FLI-1 fusion protein resulting from the t(11;22) translocation in Ewing sarcoma. *Mol. Cell Biol.* 14, 3230–3241.
 58. Dedova, I.V., Nikolaeva, O.P., Safer, D., De La Cruz, E.M., and dos Remedios, C.G. (2006). Thymosin beta4 induces a conformational change in actin monomers. *Biophys. J.* 90, 985–992. <https://doi.org/10.1529/biophysj.105.063081>.
 59. Zhang, Y., Feurino, L.W., Zhai, Q., Wang, H., Fisher, W.E., Chen, C., Yao, Q., and Li, M. (2008). Thymosin Beta 4 is overexpressed in human pancreatic cancer cells and stimulates proinflammatory cytokine secretion and JNK activation. *Cancer Biol. Ther.* 7, 419–423.
 60. Gemoll, T., Strohkamp, S., Schillo, K., Thorns, C., and Habermann, J.K. (2015). MALDI-imaging reveals thymosin beta-4 as an independent prognostic marker for colorectal cancer. *Oncotarget* 6, 43869–43880. <https://doi.org/10.18632/oncotarget.6103>.
 61. Ryu, Y.K., Lee, Y.S., Lee, G.H., Song, K.S., Kim, Y.S., and Moon, E.Y. (2012). Regulation of glycogen synthase kinase-3 by thymosin beta-4 is associated with gastric cancer cell migration. *Int. J. Cancer* 131, 2067–2077. <https://doi.org/10.1002/ijc.27490>.
 62. Cha, H.-J., Jeong, M.J., and Kleinman, H.K. (2003). Role of thymosin β4 in tumor metastasis and angiogenesis. *J. Natl. Cancer Inst.* 95, 1674–1680. <https://doi.org/10.1093/jnci/djg100>.
 63. Abal, M., Llaurado, M., Doll, A., Monge, M., Colas, E., Gonzalez, M., Rigau, M., Alazzouzi, H., Demajo, S., Castellvi, J., et al. (2007). Molecular determinants of invasion in endometrial cancer. *Clin. Transl. Oncol.* 9, 272–277.
 64. Kwartler, C.S., Chen, J., Thakur, D., Li, S., Baskin, K., Wang, S., Wang, Z.V., Walker, L., Hill, J.A., Epstein, H.F., et al. (2014). Overexpression of smooth muscle myosin heavy chain leads to activation of the unfolded protein response and autophagic turnover of thick filament-associated proteins in vascular smooth muscle cells. *J. Biol. Chem.* 289, 14075–14088. <https://doi.org/10.1074/jbc.M113.499277>.
 65. Hart, L.S., Cunningham, J.T., Datta, T., Dey, S., Tameire, F., Lehman, S.L., Qiu, B., Zhang, H., Cerniglia, G., Bi, M., et al. (2012). ER stress-mediated autophagy promotes Myc-dependent transformation and tumor growth. *J. Clin. Invest.* 122, 4621–4634. <https://doi.org/10.1172/jci62973>.
 66. Vidal, R.L., and Hetz, C. (2012). Crosstalk between the UPR and autophagy pathway contributes to handling cellular stress in neurodegenerative disease. *Autophagy* 8, 970–972. <https://doi.org/10.4161/auto.20139>.
 67. Tafe, L.J., Riggs, E.R., and Tsongalis, G.J. (2014). Lynch syndrome presenting as endometrial cancer. *Clin. Chem.* 60, 111–121. <https://doi.org/10.1373/clinchem.2013.206888>.
 68. Peltomäki, P. (2003). Role of DNA mismatch repair defects in the pathogenesis of human cancer. *J. Clin. Oncol.* 21, 1174–1179. <https://doi.org/10.1200/jco.2003.04.060>.
 69. McKenzie, R., Scott, R.J., Otton, G., and Scurry, J. (2016). Early changes of endometrial neoplasia revealed by loss of mismatch repair gene protein expression in a patient diagnosed with Lynch syndrome. *Pathology* 48, 78–80. <https://doi.org/10.1016/j.pathol.2015.11.003>.
 70. Birge, R.B., Kalodimos, C., Inagaki, F., and Tanaka, S. (2009). Crk and CrkL adaptor proteins: networks for physiological and pathological signaling. *Cell Commun. Signal.* 7, 13. <https://doi.org/10.1186/1478-811X-7-13>.
 71. Zhao, T., Miao, Z., Wang, Z., Xu, Y., Wu, J., Liu, X., You, Y., and Li, J. (2013). Overexpression of CRKL correlates with malignant cell proliferation in breast cancer. *Tumour Biol.* 34, 2891–2897. <https://doi.org/10.1007/s13277-013-0851-7>.
 72. Lin, F., Chengyao, X., Qingchang, L., Qianze, D., Enhua, W., and Yan, W. (2015). CRKL promotes lung cancer cell invasion through ERK-MMP9 pathway. *Mol. Carcinog.* 54 (Suppl 1), E35–E44. <https://doi.org/10.1002/mc.22148>.
 73. Fu, L., Dong, Q., Xie, C., Wang, Y., and Li, Q. (2015). CRKL protein overexpression enhances cell proliferation and invasion in pancreatic cancer. *Tumour Biol.* 36, 1015–1022. <https://doi.org/10.1007/s13277-014-2706-2>.
 74. Patel, N.M., Nozaki, S., Shortle, N.H., Bhat-Nakshatri, P., Newton, T.R., Rice, S., Gelfanov, V., Boswell, S.H., Goulet, R.J., Jr., Sledge, G.W., Jr., and Nakshatri, H. (2000). Paclitaxel sensitivity of breast cancer cells with constitutively active NF-kappaB is enhanced by I-kappaBalpha super-repressor and parthenolide. *Oncogene* 19, 4159–4169. <https://doi.org/10.1038/sj.onc.1203768>.
 75. Ayala, G.E., Dai, H., Ittmann, M., Li, R., Powell, M., Frolov, A., Wheeler, T.M., Thompson, T.C., and Rowley, D. (2004). Growth and survival mechanisms associated with perineural invasion in prostate cancer. *Cancer Res.* 64, 6082–6090. <https://doi.org/10.1158/0008-5472.CAN-04-0838>.
 76. Kanwal, M., Smahel, M., Olsen, M., Smahelova, J., and Tachezy, R. (2020). Aspartate beta-hydroxylase as a target for cancer therapy. *J. Exp. Clin. Cancer Res.* 39, 163. <https://doi.org/10.1186/s13046-020-01669-w>.
 77. Ko, Y.A., Jamaluddin, M.F.B., Adebayo, M., Bajwa, P., Scott, R.J., Dharmarajan, A.M., Nahar, P., and Tanwar, P.S. (2018). Extracellular matrix (ECM) activates beta-catenin signaling in uterine fibroids. *Reproduction* 155, 61–71. <https://doi.org/10.1530/rep-17-0339>.
 78. Robertson, G. (2003). Screening for endometrial cancer. *Med. J. Aust.* 178, 657–659.
 79. Hulsen, T., de Vlieg, J., and Alkema, W. (2008). BioVenn - a web application for the comparison and visualization of biological lists using

- area-proportional Venn diagrams. *BMC Genom.* 9, 488. <https://doi.org/10.1186/1471-2164-9-488>.
80. Lin, G., Chai, J., Yuan, S., Mai, C., Cai, L., Murphy, R.W., Zhou, W., and Luo, J. (2016). VennPainter: a tool for the comparison and identification of candidate genes based on Venn diagrams. *PLoS One* 11, e0154315. <https://doi.org/10.1371/journal.pone.0154315>.
81. Syed, S.M., Kumar, M., Ghosh, A., Tomasetig, F., Ali, A., Whan, R.M., Alterman, D., and Tanwar, P.S. (2020). Endometrial Axin2(+) cells drive epithelial homeostasis, regeneration, and cancer following oncogenic transformation. *Cell Stem Cell* 26, 64–80.e13. <https://doi.org/10.1016/j.stem.2019.11.012>.
82. Venkata, V.D., Jamaluddin, M.F.B., Goad, J., Drury, H.R., Tadros, M.A., Lim, R., Karakoti, A., O'Sullivan, R., Lus, Y., Jaaback, K., et al. (2022). Development and characterization of human fetal female reproductive tract organoids to understand Mullerian duct anomalies. *Proc. Natl. Acad. Sci. USA* 119, e2118054119. <https://doi.org/10.1073/pnas.2118054119>.
83. Liu, W., Xie, L., He, Y.H., Wu, Z.Y., Liu, L.X., Bai, X.F., Deng, D.X., Xu, X.E., Liao, L.D., Lin, W., et al. (2021). Large-scale and high-resolution mass spectrometry-based proteomics profiling defines molecular subtypes of esophageal cancer for therapeutic targeting. *Nat. Commun.* 12, 4961. <https://doi.org/10.1038/s41467-021-25202-5>.
84. Jamaluddin, M.F.B., Nahar, P., and Tanwar, P.S. (2018). Proteomic characterization of the extracellular matrix of human uterine fibroids. *Endocrinology* 159, 2656–2669. <https://doi.org/10.1210/en.2018-00151>.

STAR★METHODS

KEY RESOURCES TABLE

REAGENT or RESOURCE	SOURCE	IDENTIFIER
Antibodies		
Anti-MLH (M1) mouse monoclonal primary antibody	Ventana	Cat#07862237001
Anti-MSH2 (G219-1129) mouse monoclonal primary antibody	Ventana	Cat#07862253001
Anti-PMS2 (A16-4) mouse monoclonal primary antibody	Ventana	Cat#07862261001
Anti-MSH6 (SP93) rabbit monoclonal primary antibody	Ventana	Cat#07862245001
Biological samples		
Human adjacent normal endometrium and tumor samples	This paper	N/A
Chemicals, peptides, and recombinant proteins		
Sodium carbonate	Honeywell Fluka	Cat#71347; CAS: 497-19-8
Complete mini protease inhibitor cocktail	Roche	Cat#4693124001
PhosStop	Roche	Cat#4906837001
Urea	Sigma-Aldrich	Cat#51456; CAS: 57-13-6
Thiourea	Sigma-Aldrich	Cat#T7875; CAS: 62-56-6
Dithiothreitol	Sigma-Aldrich	Cat#D0632; CAS: 3483-12-3
Iodoacetamide	Sigma-Aldrich	Cat#A3221; CAS: 144-48-9
Trypsin/Lys-C Mix	Promega	Cat#V5072
Triethylammonium bicarbonate	Sigma-Aldrich	Cat#T7408; CAS: 15715-58-9
Trifluoroacetic acid	Sigma-Aldrich	Cat#T6508; CAS:76-05-1
Acetonitrile LC/MS grade	Thermo Scientific	Cat#51101; CAS: 75-05-8
Fetal bovine serum	Bovogen	Cat#SFBS-F
L-glutamine	HyClone	Cat#SH30034.01
Penicillin-streptomycin	Thermo Fisher Scientific	Cat#15070-063
Accumax	Thermo Fisher Scientific	Cat#0046656
Matrigel: Cultrex® reduced growth factor basement membrane matrix	Trevigen	Cat#3433-010-01
GlutaMAX (100X)	Thermo Fisher Scientific (Gibco)	Cat#35050-061
B27 supplement	Thermo Fisher Scientific (Gibco)	Cat#12587-010
N-2 supplement	Thermo Fisher Scientific (Gibco)	Cat#17502-048
Nicotinamide	Sigma-Aldrich	Cat#N0636; CAS:98-92-0
N-acetyl-L-cysteine	Sigma-Aldrich	Cat#A9165; CAS:616-91-1
β-Estradiol	Sigma-Aldrich	Cat#E8875; CAS:50-28-2
Human EGF recombinant	Peptotech	Cat#100-15-500
Human FGF-10	Peptotech	Cat#100-26-250
ITS liquid media supplement (100x)	Sigma-Aldrich	Cat#I3146
A83-01	Tocris/Sapphire Bioscience	Cat#S7692
TrypLE express	Thermo Fisher Scientific (Gibco)	Cat#12604-021
Y-27632 dihydrochloride	Sapphire Bioscience	Cat#S1049
DMEM/F12 HAM	Sigma-Aldrich	Cat#D8437
HBSS/Modified	HyClone	Cat#SH30031.02
HEPES solution	Sigma-Aldrich	Cat#H0887; CAS:7365-45-9
Advanced DMEM/F12	Thermo Fisher Scientific	Cat#12634-010
Critical commercial assays		
Qubit 2.0 Fluorometer Assay	Invitrogen	N/A
PrestoBlue cell viability assay	Thermo Fisher Scientific	A13261
DC Protein Assay	Biorad	Cat#5000113; 5000114

(Continued on next page)

Continued

REAGENT or RESOURCE	SOURCE	IDENTIFIER
Deposited data		
MS proteomic data – MS spectral library and SWATH data	This paper	PRIDE dataset identifier: PXD031784 Project DOI: 10.6019/PXD031784
Experimental models: Cell lines		
L-WRN cells	ATCC	Cat#CRL-3276; RRID: CVCL_DA06
Software and algorithms		
GraphPad Prism version 9.3.0	GraphPad	https://www.graphpad.com/
Protein Pilot version 4.5	Applied Biosystems MDS Sciex	https://proteinpilot.software.informer.com/4.5/
PeakView version 2.0	Sciex	https://sciex.com/products/software/peakview-software
MarkerView version 1.2	Sciex	https://sciex.com/products/software/markerview-software
Perseus version 1.6.5.0	(Tyanova et al., 2016)	https://maxquant.net/perseus/
Venny 2.1.0 (BioinfoGP)	(Oliveros, 2007)	https://bioinfoGP.cnb.csic.es/tools/venny/
Venn Painter 1.2.0	(Lin et al., 2010)	https://bio.tools/VennPainter
Ingenuity pathway analysis	Qiagen	https://analysis.ingenuity.com/pa/installer/select
Gitools version 2.3.1	(Perez-Llamas et al., 2011)	http://www.gitools.org/
Other		
Oasis PRiME HLB Cartridge 1cc/30 mg columns for peptide desalting	Waters	186008055
TSKgel Amide-80 HILIC columns packed with 3 μm particles (4.6 mm ID x 15 cm) for HILIC fractionation	Tosoh Biosciences	https://www.separations.eu.tosohbioscience.com/solutions/hplc-products/hydrophilic-interaction/tskgel-amide-80

RESOURCE AVAILABILITY

Lead Contact

Further information and requests for resources and reagents should be directed to and will be fulfilled by the Lead Contact, Prof. Pradeep Tanwar (pradeep.tanwar@newcastle.edu.au).

Materials availability

All unique/stable reagents generated in this study are available from the [Lead Contact](#) with a completed Materials Transfer Agreement.

Data and code availability

- The mass spectrometry proteomics data have been deposited to the ProteomeXchange Consortium via the PRIDE partner repository with the dataset identifier PXD031784 and 10.6019/PXD03178.
- This paper does not report original code.
- Any additional information required to reanalyze the data reported in this paper is available from the [Lead Contact](#) upon request.

EXPERIMENTAL MODEL AND SUBJECT DETAILS

Human EC tissues were collected in accordance with the guidelines of the Institutional Human Research Ethics Committee at the University of Newcastle, NSW, Australia. The tumor samples were obtained during surgical hysterectomies after obtaining informed consent from EC patients. None of the patients received any chemotherapy before surgery. The fresh tumor tissue specimens were immediately transferred to the laboratory, extensively washed with phosphate buffered saline (PBS) to remove excess blood, snap frozen, and kept in liquid nitrogen until use.⁷⁷

METHOD DETAILS

Protein extraction and digestion

Tumor tissue samples isolated from about 2 to 4 sites of EC and one adjacent normal endometrium (ANE) from each of the twenty patients (total $n = 79$, tissue samples: 63 tumors and 16 ANE samples) were subjected to protein extraction. The amount of tumor tissue collected depended on the size of the visible tumor in the uterus at the time of surgery. Tissue samples were collected immediately after the removal of the tumor from the patient body but not after the completion of the surgery, which usually takes an additional 1–4 h after the removal of the tumor, to minimize any changes in tumor protein profile. The ANE tissues had the endometrial thickness of 1–5 mm, which is clinically considered normal,⁷⁸ and were histopathologically validated by a pathologist. We also obtained patients' histopathological reports and confirmed that the ANE tissues were normal. In four patients, adjacent normal tissue was unavailable due to the extensive spread of cancer in the cavity of their uteri. To extract protein, we homogenized 10–60 mg (~4–10 mm) of tissue in ice-cold lysis buffer that contained 0.1 M Na_2CO_3 pH 11.3, protease (Sigma, St. Louis, MO, USA) and phosphatase inhibitors (Roche, Indianapolis, IN, USA) using beadbug homogenizer (Benchmark Scientific, Edison, NJ, USA) for 15 s intervals and incubated for 1 h at 4°C. We had protein yields in a range of 500–2000 μg corresponding to the size of the tumor tissue used. The soluble proteins were resuspended in urea (6M urea, 2M thiourea). Dithiothreitol (DTT) was added to a final concentration of 10 mM and samples were incubated for 30 min at room temperature. Subsequently, iodoacetamide (Sigma-Aldrich, St. Louis, MO, USA) was added to a final concentration of 20 mM and incubated for 30 min at room temperature in the dark. Lys-C/trypsin (Promega, Madison, WI, USA) was used at 1:50 ratio to protein and incubated at room temperature for 3 h. Samples were then diluted to <0.75M by the addition of 50 mM triethylammonium bicarbonate, pH 7.8 and digested overnight at 37°C. The following day, samples were cleaned up using the solid phase extraction (SPE) columns (Oasis PRIME HLB, Waters, Rydalmere, NSW Australia), and eluted with increasing concentrations of acetonitrile (Acn; 60%, 80 and 100%) in 0.1% trifluoroacetic acid. Peptide concentrations were determined using a Qubit 2.0 Fluorometer assay (Invitrogen, Eugene, OR, USA).

Library generation for SWATH analysis and LC-MS/MS acquisition

Approximately 30 μg of tryptic peptides from tumor and ANE were fractionated by hydrophilic interaction chromatography (HILIC) using a Dionex UltiMate 3000 capLC system (Dionex, Sunnyvale, CA) equipped with TSKgel Amide-80 HILIC columns packed with 3 μm particles (4.6 mm ID x 15 cm) (Tosoh Biosciences, PA, USA) connected in line. 15 fractions (SFig. 1) were collected with the following mobile phases: 0.1% TFA in HPLC water (solvent A) and 0.1% TFA in Acn (solvent B). Peptides were resolved using a 35-min linear gradient from 98% to 25% solvent B, with a constant flow of 6 $\mu\text{L}/\text{min}$. Fractions were collected into LC-MS grade glass vials (12 x 32 mm glass screw neck vial (Waters, Milford, MA USA), dried, and resuspended in 2% Acn containing 0.1% formic acid. 10 μL from each fraction was injected on the Sciex TripleTOF q6600 mass spectrometer fitted with a DuoSpray ion source (AB SCIEX) and coupled to an Agilent 1200 HPLC (Agilent, California) equipped with a trapping column (75 μm x 15 cm ChromXP, C18, 3 μm , 120 Å) and C18 RP column (ChromXP C18, 3 μm 120 Å 15 cm). Samples were run using a 70 min multi-step gradient from 5 to 98% solvent B (solvent A 0.1% formic acid in HPLC water; solvent B: 0.1% formic acid in Acn) at a flow rate of 5 $\mu\text{L}/\text{min}$. Data were acquired using floating ion spray voltage of 5.5 kV, curtain gas of 35 psi, and an interface heater temperature of 150°C. A DDA method was set up with the MS survey range set between 35 and 1250 amu followed by dependent MS/MS scans with a mass range set between 350 and 1250 amu (50 m s) of the 20 most intense ions in the high sensitivity mode with a 2⁺–5⁺ charge state inclusive. Dynamic exclusion was set for a period of 15 s.

Data files were then searched against the Uniprot human database (Swissprot, all isoforms, accessed 25/10/2018, with 42,413 entries) with Protein Pilot 4.5, with Cys alkylation set to iodoacetamide and a 95% protein confidence cutoff. The resulting protein pilot.group file was used to generate the library which was used for SWATH processing and quantification.

SWATH analysis and data processing

Tryptic peptides samples from tumors (5 μg) and ANEs (5 μg) were injected in data independent acquisition (DIA) mode for SWATH analysis. The LC gradient conditions for the SWATH experiment were the same as those used for the data dependent experiments. The mass spectrometer was operated with a 25 ms TOF MS scan followed by product ion mode of 100 variable width isolation windows covering a mass range of 400–1250, with a cycle time of 2.5 s. An overlap of 1 Da between each window was used. The SWATH analysis data were processed with PeakView 2.0 and MarkerView 1.2. For quantification using PeakView 2.0, thresholds were set at a 99% peptide confidence, 1% FDR, and the XIC width was set at 20 ppm. Modified and shared peptides were excluded, such that shared peptides were only removed from proteins confidently identified in the spectral library, removing 240 peptides (these proteins are quantified using only unique peptides). The data was exported to MarkerView, then exported as a text file. For each MS spectrum, the peaks were ranked by intensity, and the bottom peaks with less than 2.00⁴ were considered to be very low abundance and non-existence. The 2.00⁴ intensity value can be user modified, and we tested several values, with similar results. Using Perseus (1.6.5.0), the samples were log₂ transformed and median normalized. For volcano plot analysis, an FDR threshold of 0.05% and s₀ value of 0.1 were set. We used Venny 2.1.0 (BioinfoGP), BioVenn⁷⁹ and VennPainter 1.2.0⁸⁰ to create scaled or unscaled Venn diagrams respectively, illustrating the number of shared and differentially expressed proteins within each site of the EC region.

Ingenuity pathway analysis (IPA)

The list of identified EC proteins commonly found in each site within the same tumor from individual patients were further analyzed using QIAGEN's Ingenuity Pathway Analysis (IPA, QIAGEN Redwood City, CA, USA) to interpret the differentially expressed proteins in the context of predominant canonical pathways and networks. Our results in this database were measured from the following settings: (a) a p value < 0.05 (Fisher exact test) and (b) a ratio of the number of proteins in the dataset that map to the pathway divided by the total number of proteins that are present in the canonical pathway.

Mismatch repair (MMR) protein detection

We examined protein expression for MLH1, MSH2, PMS2 and MSH6 in 28 tumor tissues by immunohistochemical staining as described previously²⁴ using following antibodies (MLH1 (M1); MSH2 (G219-1129); PMS2 (EPR3947); MSH6 (44) [Ventana, AZ, USA]). The stained slides were analyzed by a pathologist. Images were captured using Olympus DP72 microscope (Olympus, Tokyo, Japan) with a 20X objective lens.

Patient-derived endometrial cancer organoids

Organoids from freshly collected tissue biopsies from four patients (16 biopsies from four patients) were developed and maintained using a published protocol.^{81,82} Briefly, fresh tumor biopsies were washed with PBS (PBS) containing 1% penicillin/streptomycin and amphotericin to remove excess blood. Tissue samples were cut into small pieces using a scalpel blade and incubated with accutax (Thermo Fisher Scientific) for 45 min at 37°C on a shaker. After the enzymatic digestion, 10% v/v fetal bovine serum (FBS) (Bovogen, VIC, AUS) was added, and the whole mixture with cells was passed through a 100 μ m cell strainer to collect epithelial cells. For organoid culture, epithelial cells (15,000 cells/well) were resuspended in 30% medium and 70% Matrigel and were placed as 50 μ L droplets in each well of a 24-well cell culture plate. All droplets were incubated at 37°C for 20 min to solidify and then overlaid with a human endometrial organoid culture medium containing 25% Wnt3A-R-spondin3-noggin conditioned media (WRN-CM) and 75% Advanced DMEM-F12, supplemented with 1% Glutamax (Thermo Fisher Scientific), 1% HEPES (Sigma), 1% penicillin-streptomycin (Thermo Fisher Scientific), 2% B27 (Thermo Fisher Scientific), 1% N2 (Thermo Fisher Scientific), 1% insulin-transferrin-selenium (Sigma), 0.2% Primocin (Invivogen, CA, USA), 50 ng/mL human EGF (Peprotech), 100 ng/mL human FGF10 (Peprotech, NJ, USA), 1.25 mM N-acetyl-L-cysteine (Sigma), 1 mM nicotinamide (Sigma), 2 nM Estrogen (Sigma), 0.5 mM A83-01 (Tocris, UK). Culture Medium was changed every 2–3 days and after 10 days of culture, organoids were harvested for further processing. Cell viability assessment was done using PrestoBlue cell viability assay (Thermo Fisher Scientific) according to the manufacturer's protocol.

QUANTIFICATION AND STATISTICAL ANALYSIS

This study involved isolating multiple tumor tissue samples from various locations of EC from a single patient (approximately 2–4 biological samples per patient). We used twenty EC patients to verify the heterogeneous nature of EC within the same patient. In total 79 biological samples ($n = 16$ ANE and $n = 63$ tumors) were subjected to LC-MS/MS. For each patient, an ANE tissue ($n = 16$ patients) was included in the LC-MS/MS analysis to identify common proteins that were only detected in EC but not in the ANE. We have collected fresh tissue samples immediately after surgical resection and before pathological analysis. For the comparison between two groups, t -tests were performed and proteins with $p < 0.05$ were considered to be statistically significant. All statistical analyses were performed using the Perseus 1.6.5.0 which is freely available from the MaxQuant website. In IPA analyses, a Fisher exact test was used to calculate a p value determining the probability that the association between the proteins in the dataset and the canonical pathway is described by chance alone. Pathways with a $p < 0.05$ were considered to be statistically significant. The sample size was determined based on previous studies,^{83,84} and no statistical method was used to predetermine sample size. Consenting adult female patients were included in the study based on pathological confirmation of endometrial cancer. No collected data were excluded from the analysis. For analysis, patients' tumor samples were stratified based on histopathological features, age, and menopausal status. For LC-MS/MS, all samples were processed and run through the mass spectrometer using the same parameters.